Modelling the solubility of gases in aqueous solutions in the context of renewable energy production with focus on geothermal plants, energy storage, and carbon sequestration

Maria Bonto[1] and Anders Andreasen[2,*]

[1] Ramboll Energy, Energy Transition, Process Department, Hannemanns Allé 53, DK-2300 København S, Denmark

[2] Ramboll Energy, Energy Transition, Process Department, Bavnehøjvej 5, DK-6700 Esbjerg, Denmark

* Corresponding author: anra@ramboll.com

Abstract

The interactions between aqueous solutions, gases, and minerals dictate the extent of issues such as scaling, degassing, and corrosion, which have a major impact on the performance of a vast number of industrial applications (e.g., geothermal plants, oil and gas production facilities, natural gas storage in saline aquifers, flue gas scrubbing, carbon sequestration, etc.). Among the different software programs available for aqueous chemistry calculations, PHREEQC and Reaktoro were tested and validated against a wide dataset of gas solubility measurements. For the datasets considered, the two programs essentially led to the same outcome with only a few discrepancies observed. Yet, the agreement between the models and experimental data was greatly affected by the selected database. The models implemented in PHREEQC and Reaktoro were also compared with the experimental bubble point pressure of fluids sampled at several geothermal wells. The satisfactory performance of both PHREEQC and Reaktoro for describing different chemical systems at a wide range of pressures and temperatures showcases their versatility and practicality for assisting in the design and optimization of various processes relevant to the energy transition (e.g., geothermal exploitation, CO_2 /H_2 transport and storage).

Keywords: gas solubility, brine chemistry, geothermal fluid, degassing, bubble point pressure estimation

1 Introduction

The design and operation of a geothermal plant are heavily impacted by the phase behavior of the fluids extracted from the subsurface. The phase behavior of the aqueous fluid is a function of its composition and pressure & temperature conditions. Deep geothermal fluids are often highly saline (>6 M) and contain dissolved gases (e.g., CO_2, CH_4, N_2). Any change in pressure and temperature across the geothermal loop will disturb the existing equilibrium conditions, triggering mineral precipitation and gas exsolution until a new equilibrium is achieved. Thus, while at the high pressures within the subsurface the geothermal fluid may be found in a single (liquid) phase, once the fluid is brought to the lower pressures at or near the surface, it may eventually split into two phases [1] (gas/liquid, liquid/solid) or even three phases (solid/liquid/gas). This may also take place in the wellbore. For some geothermal power plants, this is part of the working principle when the geothermal fluid has a sufficiently high temperature, such as the single flash plant, double flash plant [2]. For other types of plants that do not utilize flashing of the geothermal brine, e.g., the binary plant [2], any flashing is undesired.

For a given temperature and composition, the pressure at which the first bubble of gas appears is called the bubble point pressure. Operating in a two-phase regime is usually undesired and can be avoided if the bubble point pressure is known. The amount of gas released from the aqueous solution upon pressure or temperature shifts impacts the aqueous chemistry and thermophysical properties of the geothermal mixture. For instance, the release of CO_2 from the brine increases the pH, which promotes scaling. Changes in the gas-liquid-ratio (GLR) in a two-phase system alter the fluid density, specific heat,

https://doi.org/10.26434/chemrxiv-2023-4hgnm ORCID: https://orcid.org/0000-0003-0475-323X Content not peer-reviewed by ChemRxiv. License: CC BY 4.0

viscosity, and thermal conductivity, all of them important for the design of relevant equipment within the geothermal plant (e.g., pumps, heat exchangers) [3].

There are different ways of dealing with gas break-out in single/two-phase type geothermal surface facilities. The first obvious solution is to keep the pressure at the topside facilities above the bubble point pressure of the geothermal brine and thereby completely avoid degassing. However, given that the bubble point pressure might be several tens of bars, it increases the cost of the surface facilities due to the correspondingly higher design pressure of the piping and equipment required. The topside facilities can also be designed to handle gases formed by flashing/exsolution, e.g., selecting pumps that can manage a certain gas fraction, or the gases are separated, compressed, and reinjected along with the cooled geothermal brine. A third solution is to separate and vent the gases. Yet, this increases the carbon footprint due to the venting of CO_2 directly and/or from associated methane emissions if methane is present as a dissolved gas. Gases can also be oxidized/flared, converting methane to CO_2, which reduces the global warming potential (GWP) of the emissions due to a lower GWP of CO_2 compared to methane. Nonetheless, greenhouse gas emissions are still higher compared to non-venting/flaring. Lastly, gases can also be used for energy production by e.g., combustion in a gas engine or similar, provided that the heating value / Wobbe Index is sufficiently high. The exhaust from such combustion also has associated emissions of CO_2 and GWP.

Given the relevance of brine chemistry, degassing, and mineral precipitation on the design, operating philosophy, maintenance requirement, efficiency and general performance of the geothermal plant, a good knowledge of the geothermal fluid's chemical composition and phase envelope is required. Thus, fluid sampling should be performed early in the project. The chemical analysis of the samples (e.g., brine, brine-gas mixtures) can then be fed into geochemical/aqueous speciation models, which not only allow predicting the extent of gas solubility in brines and the potential for scaling as pressure and temperature shift, but also provide essential input to corrosion models. Sampling should also be carried out periodically throughout the lifetime of the geothermal plant for monitoring purposes; any shift in the chemistry conditions identified during the monitoring routine can then be used to update the models, ensuring reliable predictions.

Since scaling, corrosion, and degassing pose negative effects on a plethora of industrial applications, many different computer tools (e.g., EQ3NR [4], MINTEQA2 / Visual Minteq [5], PHREEQC [6], Reaktoro [7], the extended UNIQUAC model by García et al. [8] and the Søreide and Whitson's modified Peng-Robinson equation of state [9] for prediction of gas solubilities in brine as a few relevant examples) have been developed to describe mathematically and predict these issues under variable conditions. In the present work, PHREEQC and Reaktoro are used due to their availability (freeware / open source) and widespread usage across different disciplines (e.g., environment/ground water, petroleum, energy, etc.) for calculations involving interactions and equilibria in systems containing gases and aqueous solutions with different electrolytes. For PHREEQC, several validation studies [10]–[12] have been carried out in the context of different applications. While individual and binary-pairs gas solubilities have been calculated with PHREEQC and validated against experiments, modelling the mutual solubility of ternary gas mixtures including bubble point prediction and validation against experimental data is very limited.

The objective of this work is to validate and compare PHREEQC and Reaktoro and some of the available databases distributed freely with the software. We do this by systematically comparing the models implemented in both software programs against gas solubility measurements reported in the literature. The models are later used to assess the potential and extent of geothermal fluids degassing at different pressure and temperature conditions. Being able to predict the bubble point pressure of geothermal brine is pivotal for either selecting a sufficiently high operating and design pressure of the surface facilities or appropriately designing the surface facilities to handle any gases formed during

https://doi.org/10.26434/chemrxiv-2023-4hgnm **ORCID:** https://orcid.org/0000-0003-0475-323X Content not peer-reviewed by ChemRxiv. **License:** CC BY 4.0

operation. For the latter, quantifying the amount of gas formed is essential as well as knowing the composition of the formed gas phase.

2 Methods

In this work, the software programs PHREEQC v3 [6] and Reaktoro [7] are used. The PHREEQC v3 computer program is written in the C/C++ programming language and is designed to perform a wide variety of aqueous geochemical calculations and is delivered free of charge by the U. S. Geological Survey. The program is interfaced from the Python programming language v3.9. The chemical systems simulated in this work are modelled using the databases "phreeqc.dat" and "pitzer.dat". The Pitzer database is the PHREEQC version of the Yucca Mountain EQ3/6 thermodynamic database. Further description of the methods and models implemented in PHREEQC, including databases, is readily available and can be found in numerous relevant publications e.g., [10], [11], [13]–[15]. Reaktoro is an open-source software program developed in C++ and Python for modelling reactive processes. Reaktoro simulations were carried out using Python v3.9. Reaktoro supports many different databases, including those developed for PHREEQC. Compared to PHREEQC, where the thermodynamic models for the aqueous and gaseous phases are linked directly to a specific database, Reaktoro allows choosing the thermodynamic models for the gas and aqueous phases independently of the selected database. Moreover, Reaktoro has also a broader range of models for calculating both activity coefficients and fugacities.

To compare and test the agreement between Reaktoro and PHREEQC, "phreeqc.dat" and "pitzer.dat" were used as databases. For the model implementation in Reaktoro, where the database does not constrain the selection of the thermodynamic models for the aqueous and gas phases, the "DebyeHuckelPHREEQC" and "ActivityModelPitzer" were used as thermodynamic models for the aqueous phase with the "phreeqc.dat" and "pitzer.dat" databases, respectively. For the gas phase, the Peng Robinson model as developed in PHREEQC (i.e., "ActivityModelPengRobinsonPhreeqc") was selected. These models were chosen to ensure consistency, as mixing a thermodynamic database developed for a specific electrolyte model with a different model for activity coefficient estimation may lead to incoherent predictions.

Models simulating the solubility of gases from single (i.e., CH_4, N_2, H_2S, O_2, CO_2, H_2) and binary gas systems (CO_2-CH_4 and CO_2-N_2) in water and aqueous solutions are implemented in both PHREEQC and Reaktoro. The results from these models are compared and assessed against experimental measurements available in the literature. Within the phreeqc and pitzer databases, some gases are defined as either coupled or decoupled from redox processes. In the former case, the gases, once dissolved, can be reduced/oxidized to other aqueous species. For instance, dissolved nitrogen, $N_{2,(aq)}$, could further evolve to NH_4^+ species. These redox processes are deemed to be considerably slower and kinetically driven and, therefore, neglected in this study. Thus, when available, the definition of the gases uncoupled from redox processes is used in the implemented PHREEQC and Reaktoro models.

After validating both PHREEQC and Reaktoro against gas solubility measurements, further modelling is carried out to predict the bubble point pressure of geothermal fluids. The models can only be assessed against an experimental bubble point pressure measurement when the following conditions are reported: temperature, aqueous & gas compositions, GLR, and the pressure & temperature at which the GLR was determined. The measured GLR is typically reported at standard conditions (i.e., 1 atm and 273.15 K) [16]. Only by knowing these parameters, the composition and amount of both the gas and liquid phases can be fully defined. Studies that report the entire set of conditions required for performing the modelling are, however, scarce. To estimate the bubble point pressure, we first defined the aqueous solution with a given composition. This solution was then equilibrated with a gas phase at a specific temperature and different pressures. Upon equilibration, the composition of the gas and aqueous phase changes. As pressure increases, the volume of the gas phase decreases both because of the gas compressibility and the increased solubility of the gas phase components in the aqueous solution. The

https://doi.org/10.26434/chemrxiv-2023-4hgnm ORCID: https://orcid.org/0000-0003-0475-323X Content not peer-reviewed by ChemRxiv. License: CC BY 4.0

pressure value that yields a gas phase volume below 1×10^{-5} L (per 1 L of solution) is annotated as the bubble point pressure. In each simulation run, the pressure was increased by 0.1 bar. In PHREEQC, we defined the gas phase as a fixed pressure "GAS_PHASE" with the volume calculated from the GLR. The number of moles of gas included in the gas-liquid equilibration was then calculated internally by PHREEQC from the pressure, volume, and temperature. In Reaktoro, the number of moles of gas considered in the equilibration can be defined directly; these were calculated from the gas phase volume at standard conditions.

3 Results

3.1 Single-component gas solubility

The gas solubility predicted with PHREEQC and Reaktoro is first shown for single-component gas systems, such as CH_4, N_2, H_2S, O_2, CO_2, and H_2. The gathered experimental datasets and the modelling results are presented hereafter.

3.1.1 Methane

The models are initially compared against the experimental data from Stoessel and Byrne [17]. In these experiments, the authors measured the solubility of methane at 25ºC at moderate pressures (24-51 bar) in aqueous solutions containing different salts (e.g., NaCl, $CaCl_2$, Na_2CO_3). The amount of gas dissolved was calculated from the total gas volume and pressure change in the gas phase upon equilibration with the aqueous phase by using the ideal gas law. Figure 1 shows the performance of PHREEQC and Reaktoro for predicting the solubility of methane in NaCl (panel a), KCl (panel b), $CaCl_2$ (panel c), $MgCl_2$ (panel d), Na_2CO_3 (panel e), K_2CO_3 (panel f), $MgSO_4$ (panel g) using both pitzer and phreeqc databases. The results obtained with the two software programs are primarily identical when the same database is applied. Discrepancies between PHREEQC and Reaktoro were only observed when using phreeqc.dat for describing the methane solubility in $MgSO_4$ and Na_2CO_3 aqueous solutions. Moreover, with the pitzer database, the solubility of methane in electrolyte solutions of increasing ionic strength was not predicted correctly by neither PHREEQC nor Reaktoro.

https://doi.org/10.26434/chemrxiv-2023-4hgnm **ORCID:** https://orcid.org/0000-0003-0475-323X Content not peer-reviewed by ChemRxiv. **License:** CC BY 4.0

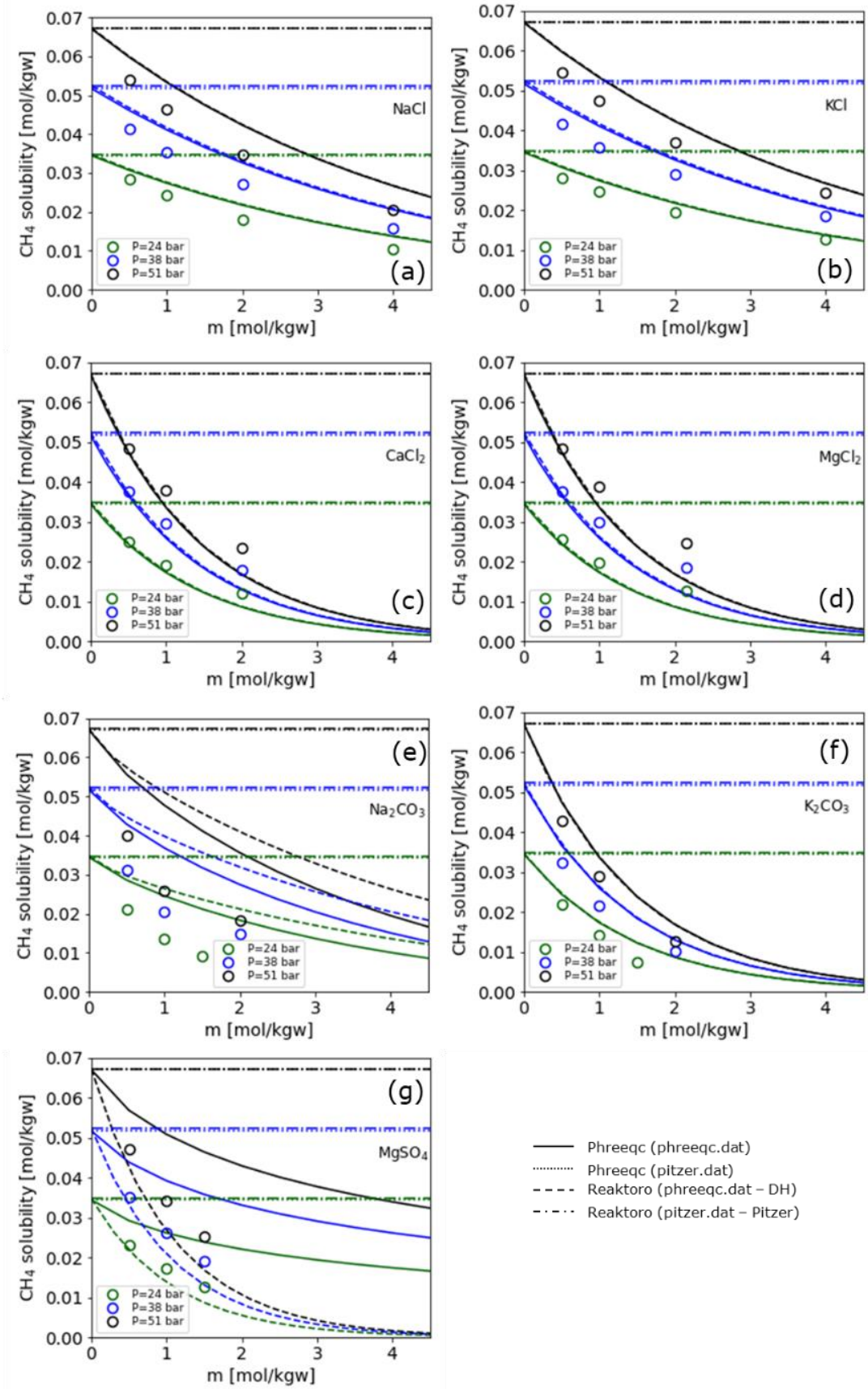

Figure 1. Solubility of methane at 25ºC and three different pressures in electrolyte solutions containing (a) NaCl, (b) KCl, (c) $CaCl_2$, (d) $MgCl_2$, (c) Na_2CO_3, (f) K_2CO_3, and (g) $MgSO_4$. Markers represent experimental data from [17] and the lines represent the prediction of the models.

https://doi.org/10.26434/chemrxiv-2023-4hgnm **ORCID:** https://orcid.org/0000-0003-0475-323X Content not peer-reviewed by ChemRxiv. **License:** CC BY 4.0

The models are also compared against experimental data obtained at higher temperatures and pressures. O'Sullivan and Smith [18] measured the solubility of methane in water and NaCl solutions (1 and 4 molal) up to 125ºC and 600 atm. Figure 2 shows the predictions of the Reaktoro and PHREEQC models against the experimental measurements obtained at a fixed temperature and increasing pressures (panels a to c) and at a fixed pressure and increasing temperatures (panel d). Using the phreeqc database, both Reaktoro and PHREEQC satisfactorily predict the solubility of methane.

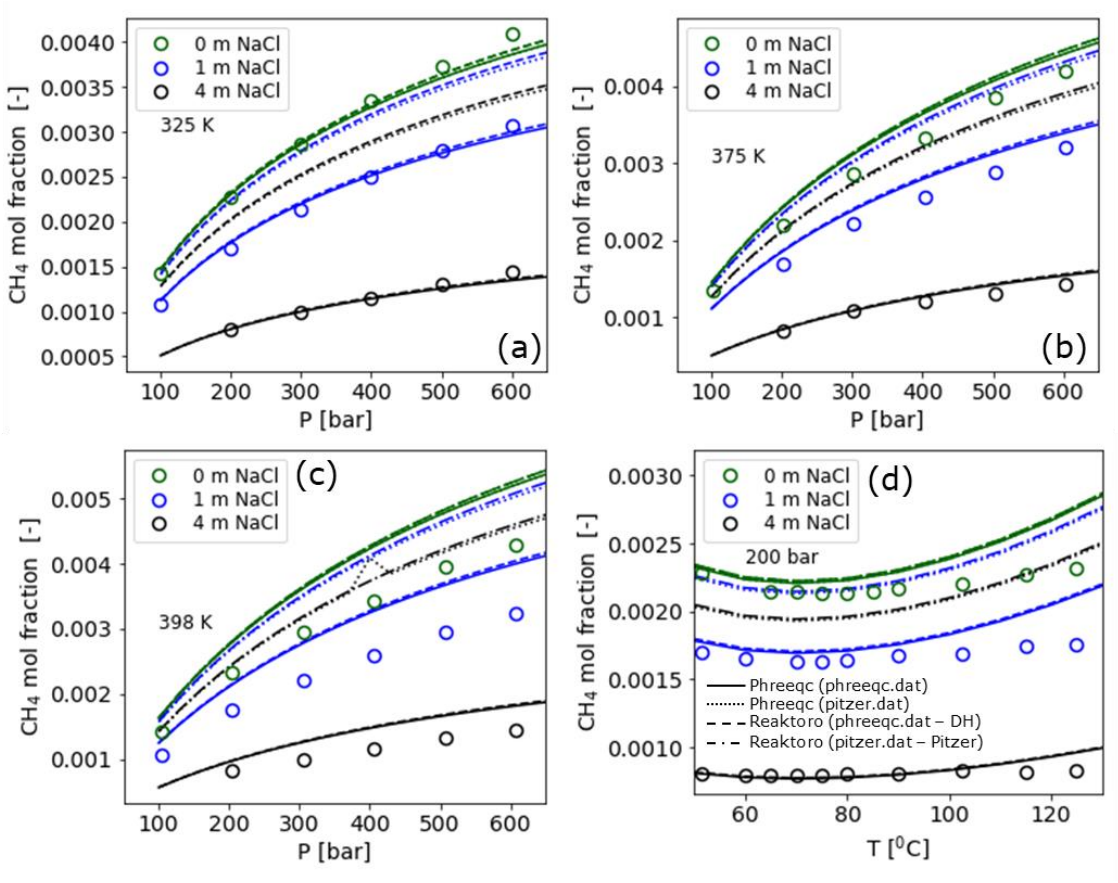

Figure 2. Solubility of methane in water and NaCl aqueous solutions at high pressures and (a) 325 K, (b) 375 K, and (c) 398 K. (d) Solubility of methane in water and NaCl aqueous solutions between 50 and 125ºC at 200 bar. Markers represent the experimental data from [18] and the lines represent the prediction of the models.

3.1.2 Nitrogen

O'Sullivan and Smith [18] also determined the solubility of nitrogen in water and NaCl aqueous solutions between 50 to 125ºC and pressures up to 600 bar. Figure 3 shows the performance of the models along with the experimental data obtained at three different temperatures. Considering "phreeqc.dat", both Reaktoro and PHREEQC lead to analogous results. In pure water, phreeqc.dat and pitzer.dat provide the same results and the discrepancy between the two databases becomes obvious only at higher ionic strength. Analogous to methane, with the pitzer database, the effect of salinity on the solubility is not properly reflected.

https://doi.org/10.26434/chemrxiv-2023-4hgnm ORCID: https://orcid.org/0000-0003-0475-323X Content not peer-reviewed by ChemRxiv. License: CC BY 4.0

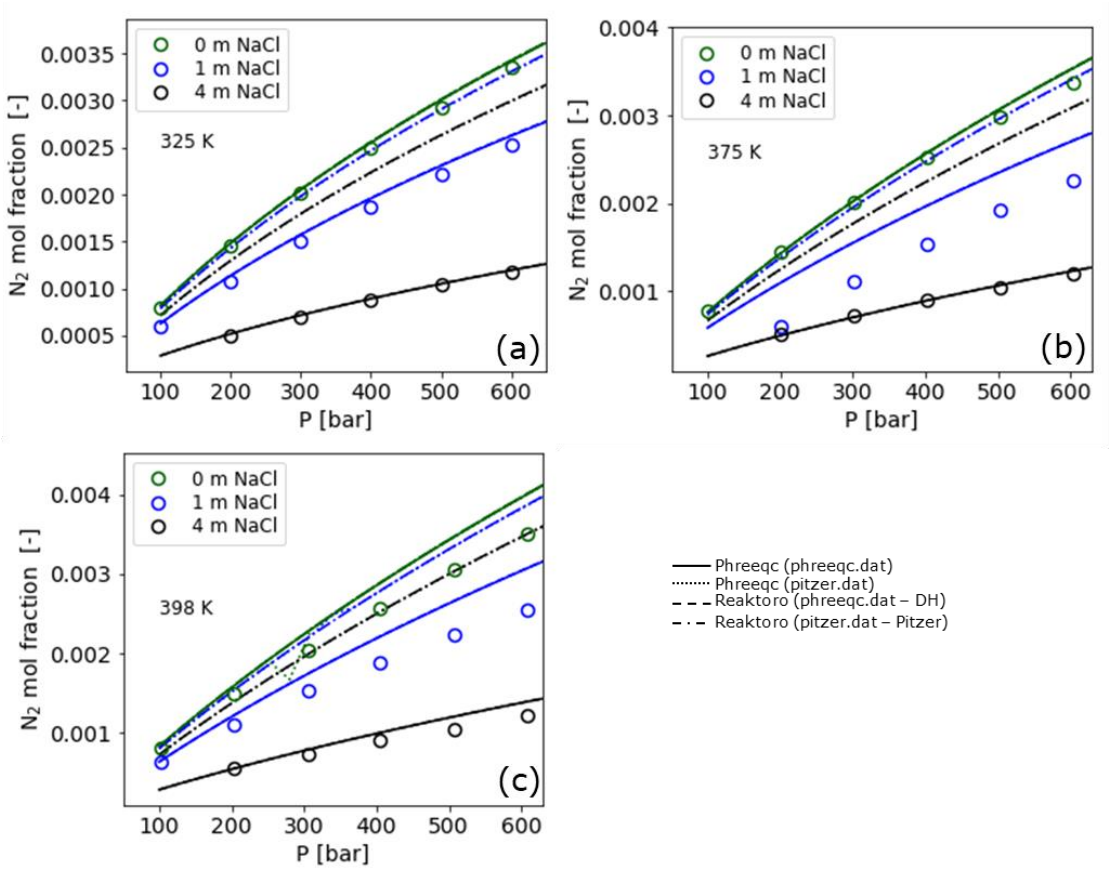

Figure 3. Solubility of nitrogen in water and NaCl aqueous solutions at high pressures and (a) 325 K, (b) 375 K, and (c) 398 K. Markers represent the experimental data from [18] and the lines represent the prediction of the models.

3.1.3 Hydrogen sulfide

Xia et al. [19] measured the solubility of H_2S in electrolytes (e.g., Na_2SO_4, NaCl) of different ionic strengths up to 100 bar and 120ºC. They measured the solubility by adding a known amount of gas to a cell containing a controlled amount of electrolyte. The amount of solution was slowly increased until the gas was completely dissolved in the liquid phase. After equilibration, very small amounts of the liquid mixture were removed to promote degassing. The pressure leading to a small gas bubble was recorded as the required equilibrium pressure to dissolve the known loaded amount of hydrogen sulfide. Figure 4 shows the performance of the models against the experimental data from Xia et al. [19]. For these experimental conditions, both Reaktoro and PHREEQC satisfactorily predict the solubility of H_2S.

https://doi.org/10.26434/chemrxiv-2023-4hgnm ORCID: https://orcid.org/0000-0003-0475-323X Content not peer-reviewed by ChemRxiv. License: CC BY 4.0

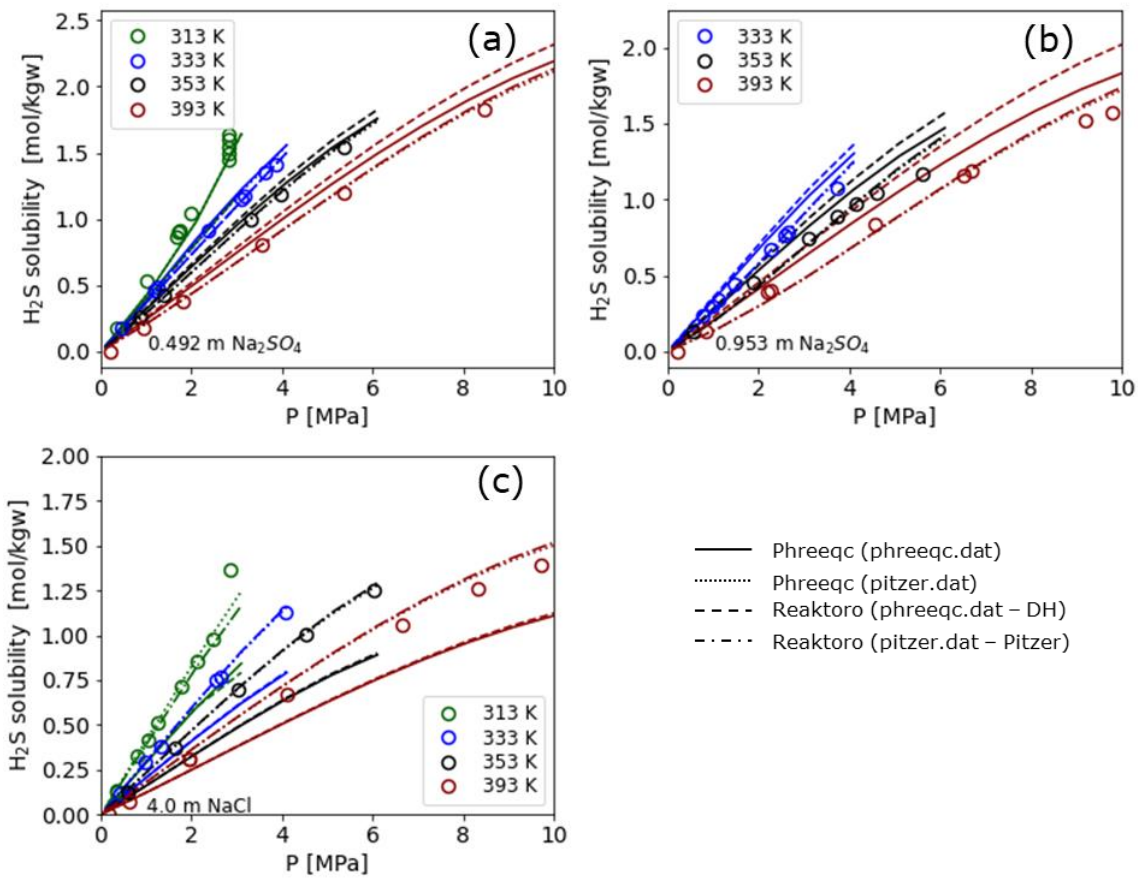

Figure 4. Solubility of H_2S at different temperatures and pressures in aqueous solutions containing (a) 0.492 m Na_2SO_4, (b) 0.953 m Na_2SO_4, and (c) 4.0 m NaCl. Markers represent the experimental data from [19].

3.1.4 Carbon dioxide

PHREEQC and Reaktoro were also tested against CO_2 solubility measurements in both water and NaCl solutions up to 400 bar and 150ºC [20]. Figure 5 shows the performance of the models against the solubility measured in water (panel a), 1 m NaCl (panel b), and 4 m NaCl (panel c). In pure water, both the pitzer and the phreeqc databases yield the same results. Yet, as the ionic strength increases, only the pitzer database, which includes interaction parameters between the CO_2 and the Na^+ satisfactorily predicts the solubility of CO_2.

https://doi.org/10.26434/chemrxiv-2023-4hgnm **ORCID:** https://orcid.org/0000-0003-0475-323X Content not peer-reviewed by ChemRxiv. **License:** CC BY 4.0

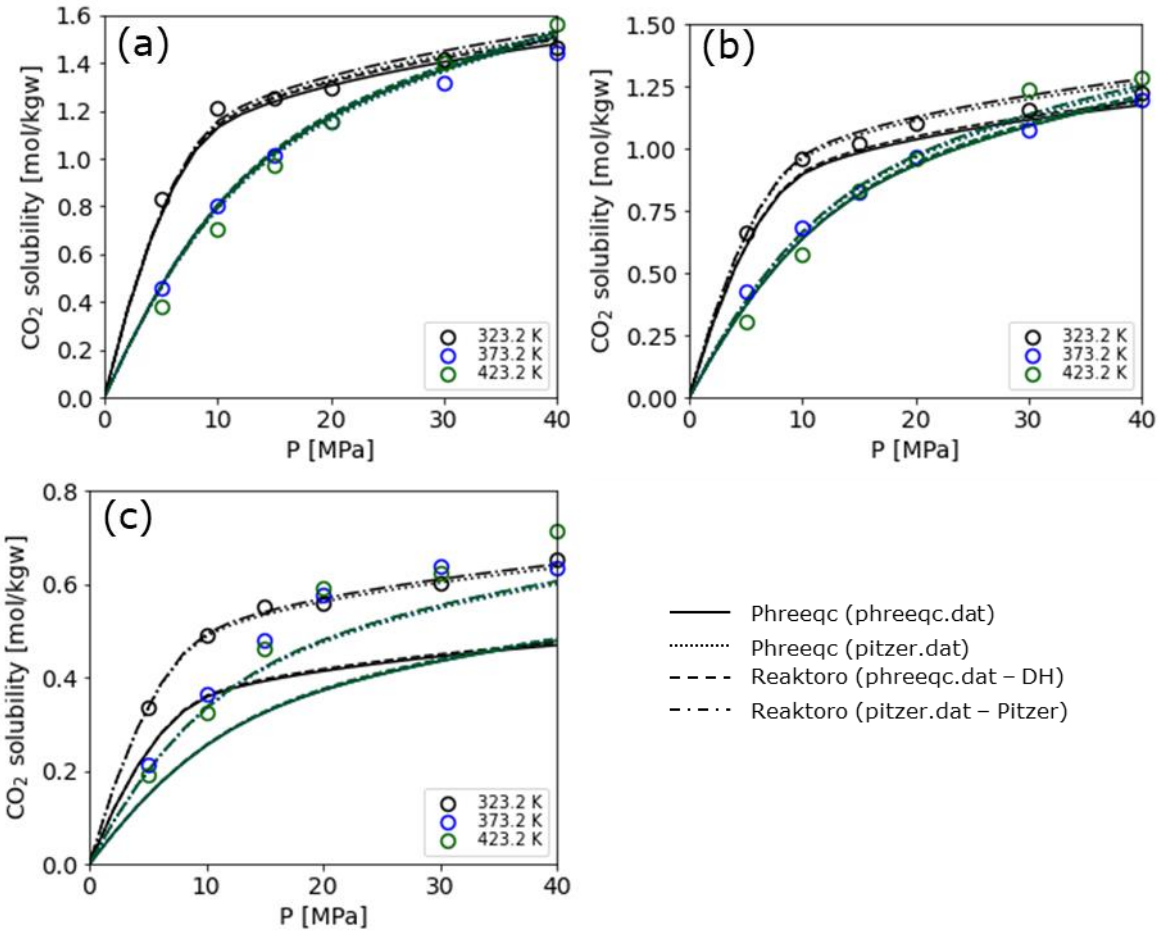

Figure 5. Solubility of CO_2 at different temperatures and pressures in (a) water and aqueous solutions containing (b) 1 m and (c) 4.0 m NaCl. The markers represent the experimental data from [20].

3.1.5 Hydrogen

Chabab et al. [21] measured the solubility of hydrogen in water and NaCl aqueous solutions up to 250 bar and 100ºC. The performance of the models against the experimental data is shown in Figure 6 for water (panel a), 1 m (panel b), 3 m (panel c), and 5 m (panel d) NaCl aqueous solutions. Using "phreeqc.dat", Reaktoro and PHREEQC lead to a very good prediction of the H_2 solubility in both water and high NaCl aqueous solutions, whereas with "pitzer.dat", at high salinity, the discrepancy between the models and the experimental data increases.

https://doi.org/10.26434/chemrxiv-2023-4hgnm ORCID: https://orcid.org/0000-0003-0475-323X Content not peer-reviewed by ChemRxiv. License: CC BY 4.0

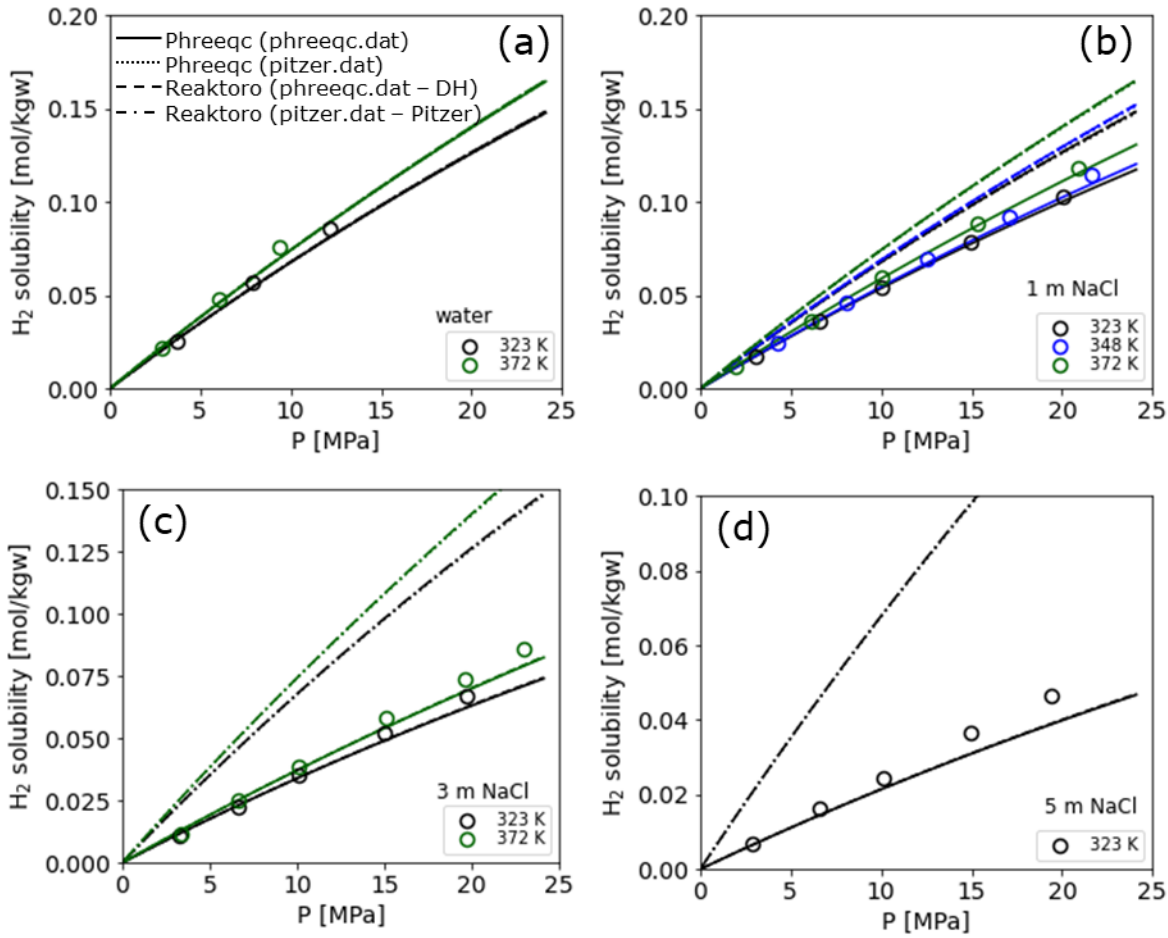

Figure 6. Solubility of H_2 at different temperatures and pressures in (a) water and aqueous solutions containing (b) 1 m, (b) 3 m, and (c) 5.0 m NaCl. Markers represent the experimental data from [21].

3.1.6 Oxygen

Chabab et al. [22] measured the solubility of oxygen up to 350 bar and 100ºC in water and NaCl aqueous solutions. Figure 7 shows the models' prediction along the solubility measurements in water (panel a), 1 m (panel b), and 4 m NaCl (panel c). Analogous to H_2, PHREEQC and Reaktoro predict correctly the solubility of oxygen at high salinity only when "phreeqc.dat" is used.

https://doi.org/10.26434/chemrxiv-2023-4hgnm ORCID: https://orcid.org/0000-0003-0475-323X Content not peer-reviewed by ChemRxiv. License: CC BY 4.0

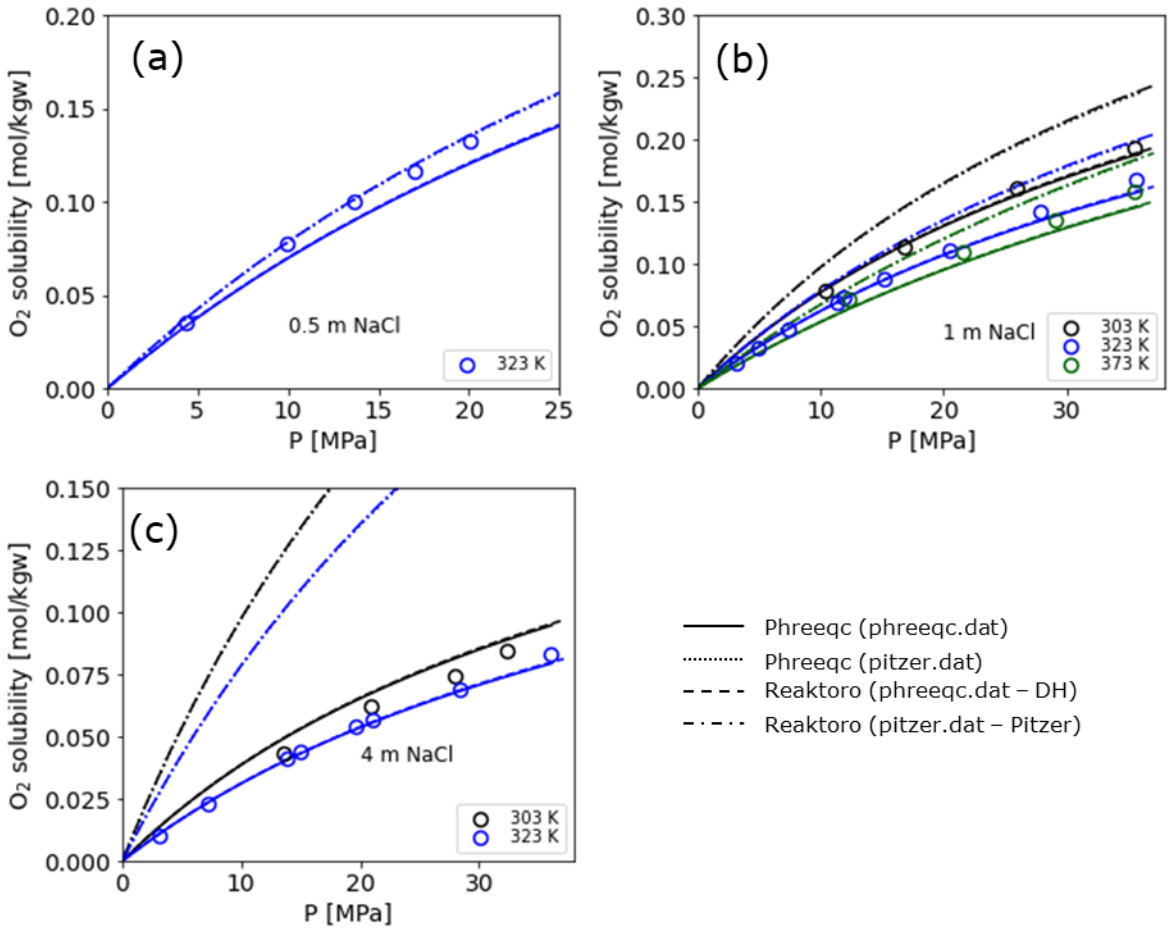

Figure 7. Solubility of O_2 at different temperatures and pressures in aqueous solutions containing (a) 0.5 m, (b) 1 m, and (c) 4.0 m NaCl. Markers represent the experimental data from [22].

3.2 Binary gas mixture solubilities

PHREEQC and Reaktoro are also compared and assessed against experimental data obtained with binary gas systems consisting of CO_2-N_2 and CO_2-CH_4 mixtures.

3.2.1 Carbon dioxide – Nitrogen

Liu et al. [23] measured the co-solubility of CO_2 and N_2 in water and aqueous solutions with a 5 wt.% salt mixture containing an equal mass of NaCl, KCl, and $CaCl_2$ up to 160 bar and 50ºC. The total amount of N_2 and CO_2 in the liquid sample was calculated from the measured temperature, pressure, and volume using the Peng-Robinson equation of state, whereas the composition of the gas phase was determined using a gas chromatogram. Figure 8 shows the experimental and modelled solubility of CO_2 (panels a, c, and e) and N_2 (panels b, d, f) against the equilibrium gas partial pressures at three different total pressures. Both the experimental and calculated molar fractions of CO_2 and N_2 in the gas phase (e.g., y_{CO2} and y_{N2}) are expressed on a "water-free" basis, i.e., the water content in the gas phase is considered negligible.

https://doi.org/10.26434/chemrxiv-2023-4hgnm ORCID: https://orcid.org/0000-0003-0475-323X Content not peer-reviewed by ChemRxiv. License: CC BY 4.0

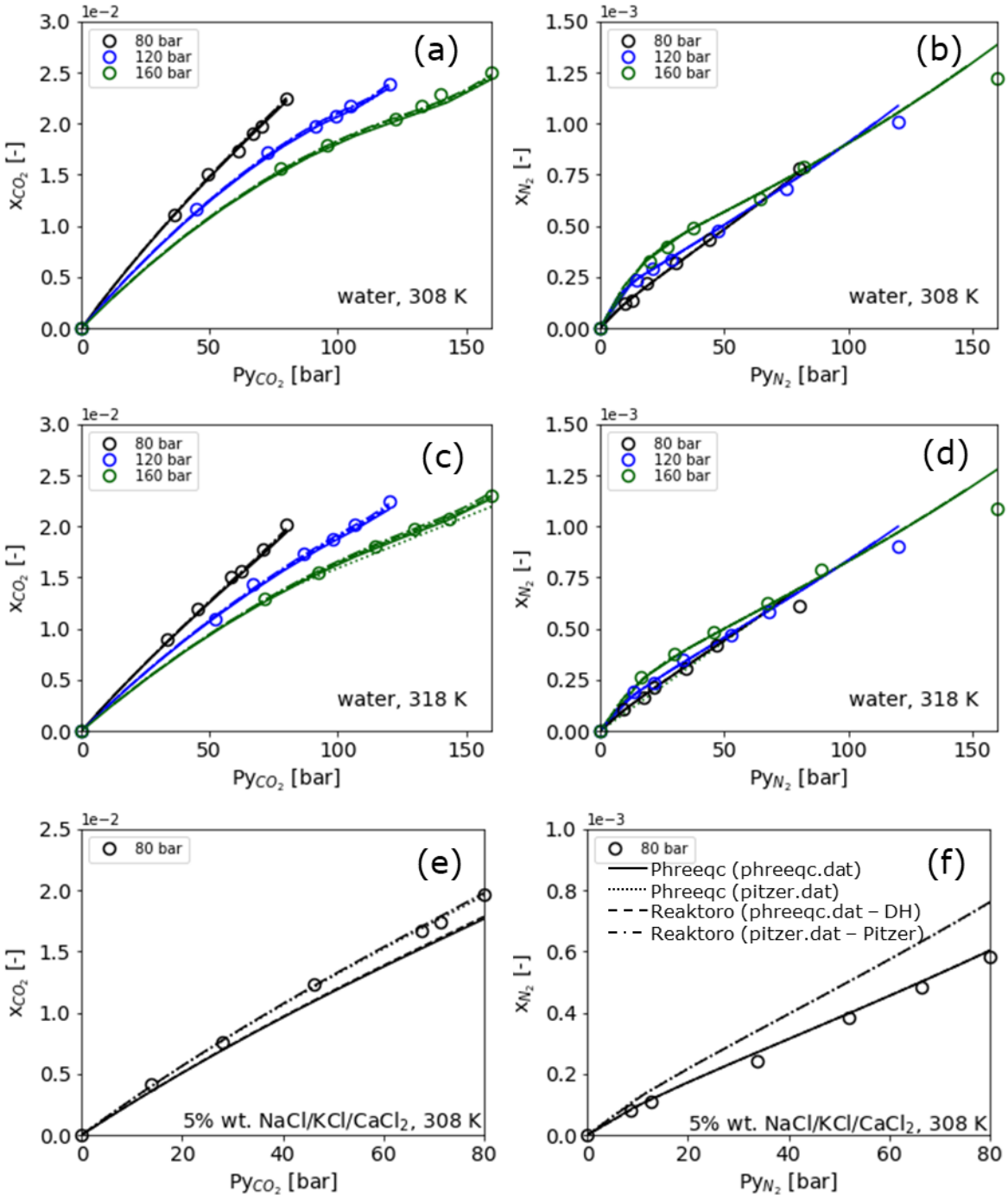

Figure 8. Co-solubility of CO_2 (panels a, c, e) and N_2 (panels b, d, f) in water (panels a→ d) and aqueous solutions (panels e and f) at different pressures and temperatures. Note that the x-axis represents the gas partial pressure of either CO_2 or N_2 upon equilibration. Markers represent the experimental data from [23].

Hassanpour et al. [24] measured the co-solubility of CO_2 and N_2 in water and brines at different pressures and temperatures. The experiments were performed with three gas phase systems simulating the composition of typical flue gas streams containing different CO_2/N_2 ratios. For each gas system, N_2 and CO_2 were injected into a cell containing water/brines at a specific molar ratio and were left to mix until the pressure and the temperature within the cell stabilized. Gas samples were also taken and analyzed by GC to confirm the desired gas composition. The CO_2/N_2 aqueous molar fraction was calculated from the material balance, i.e., by considering the initial gas composition and the final gas composition upon equilibration. The moles in the gas phase upon equilibration were calculated using

https://doi.org/10.26434/chemrxiv-2023-4hgnm ORCID: https://orcid.org/0000-0003-0475-323X Content not peer-reviewed by ChemRxiv. License: CC BY 4.0

pressure, temperature, and volume measurements and the compressibility factor using CPA-SRK72 EOS. Figure 9 shows the CO_2 (panels a, c, e) and N_2 (panels b, d, f) solubility in water at total gas pressures up to 250 bar and 30ºC.

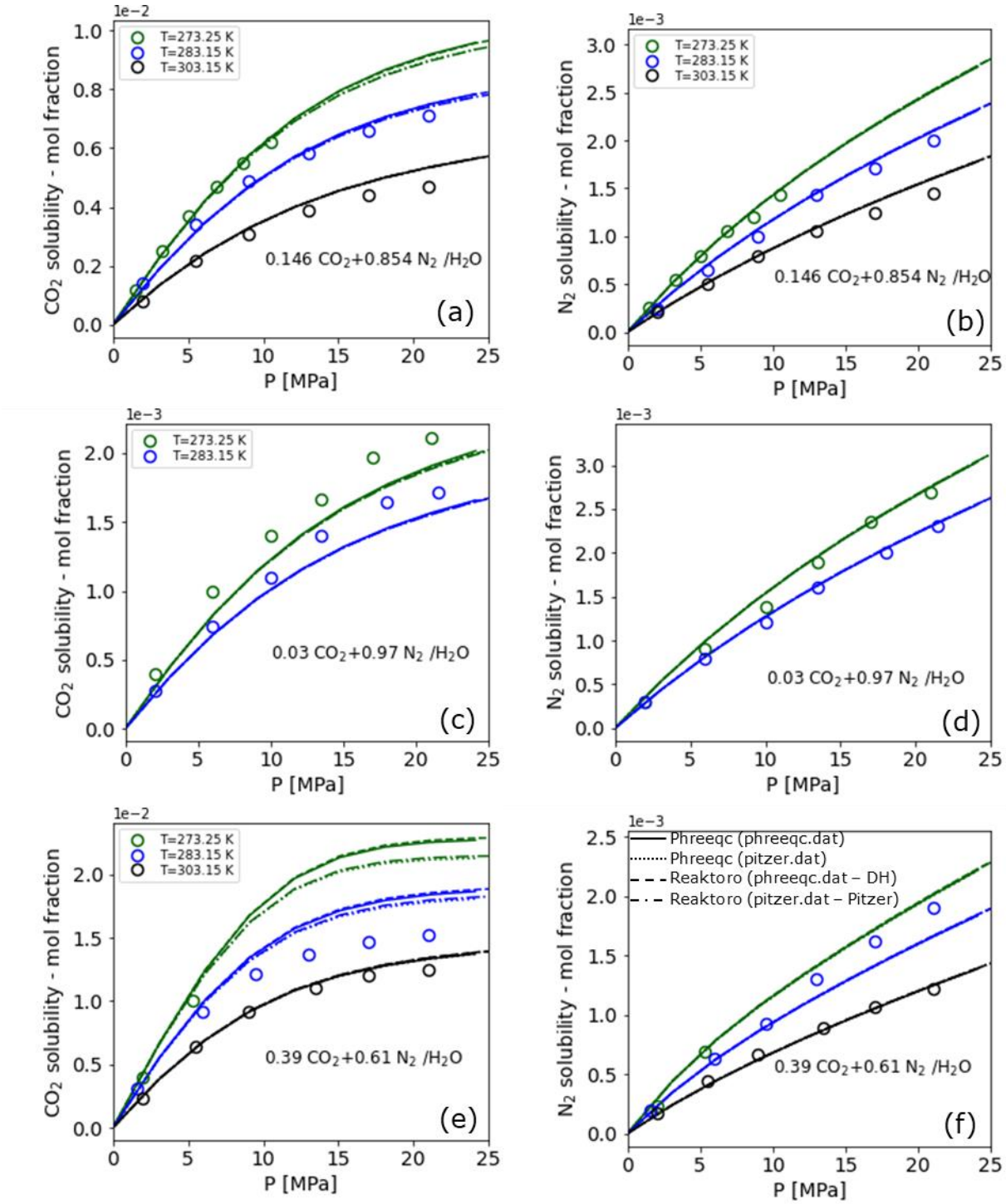

Figure 9. Co-solubility of CO_2 (panels a, c, e) and N_2 (panels b, d, f) in water at different pressures and temperatures. An initial gas phase of three different CO_2/N_2 mixtures was considered, i.e., 0.146/0.854 (panels a and b), 0.03/0.97 (panels b and c), and 0.39/0.61 (panels e and f).

For each equilibrated system, Hassanpour and coauthors [24] reported also the composition of the gas phase upon equilibration. Both in the experiments and models, the water content of the gas phase was considered negligible. Figure *10* shows the consistency between the experimental and modelled

https://doi.org/10.26434/chemrxiv-2023-4hgnm **ORCID:** https://orcid.org/0000-0003-0475-323X Content not peer-reviewed by ChemRxiv. **License:** CC BY 4.0

composition of CO_2 (panels a, c, e) and N_2 (panels b, d, f) in the gas phase for systems containing three different CO_2/N_2 mixtures.

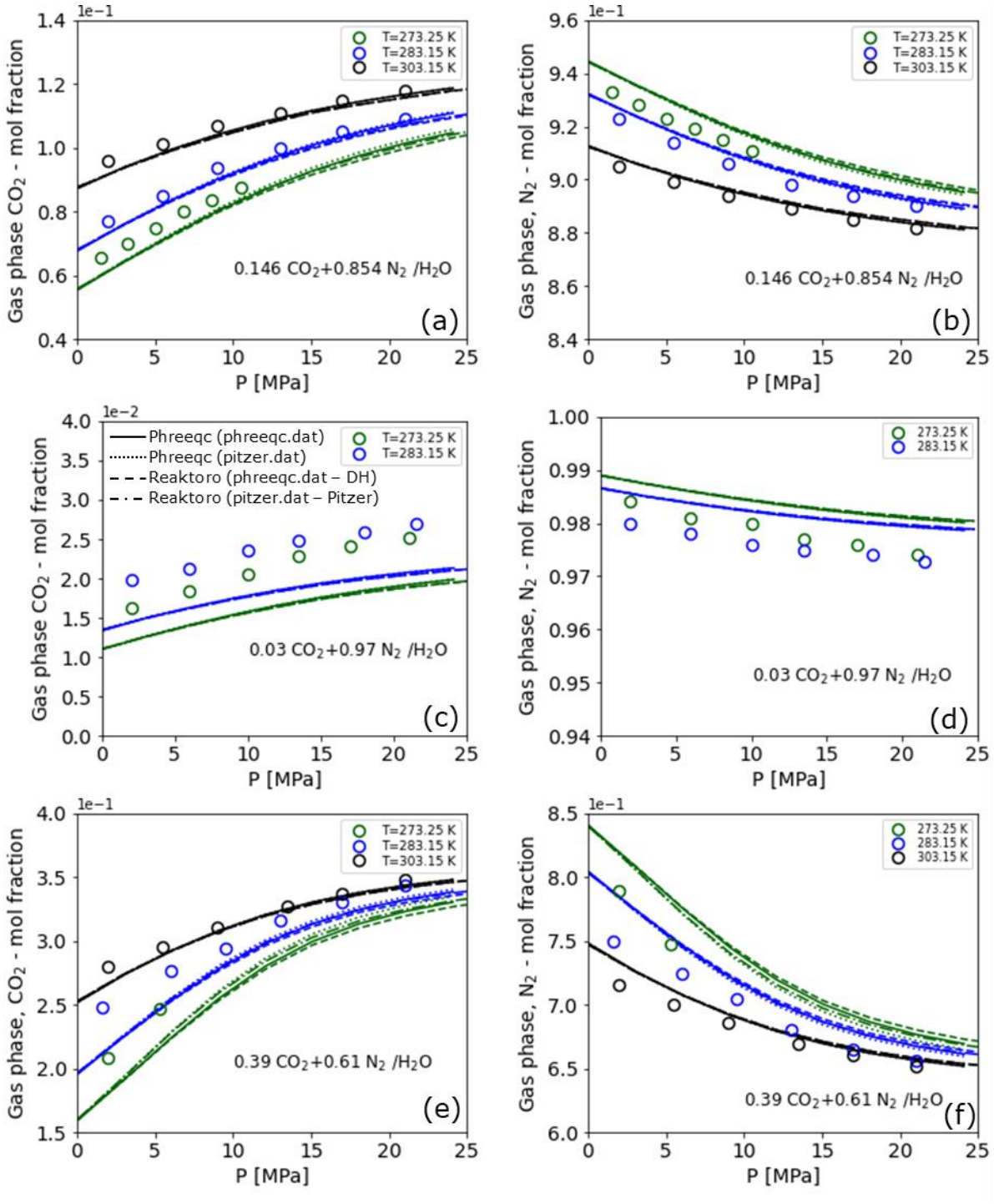

Figure 10. CO_2 (panels a, c, e) and N_2 (panels b, d, f) mol fractions in a CO_2/N_2 gas phase mixture upon equilibration with water at different pressures and temperatures. Before equilibration, the gas phase consisted of 0.146/0.854 (panels a and b), 0.03/0.97 (panels c and d), and 0.39/0.61 (panels e and f) CO_2/N_2.

Besides the solubility measurements in water, the co-solubility of CO_2 and N_2 was measured also in three different NaCl solutions (i.e., 5, 10, and 15% wt.). Before equilibration, the gas phase contained 14.6% (mol) CO_2 and 85.4% N_2. Figure 11 shows the measured and predicted CO_2 (panels a, c, e) and N_2 (panels b, d, f) solubility in the three brines at different pressures and temperatures.

https://doi.org/10.26434/chemrxiv-2023-4hgnm ORCID: https://orcid.org/0000-0003-0475-323X Content not peer-reviewed by ChemRxiv. License: CC BY 4.0

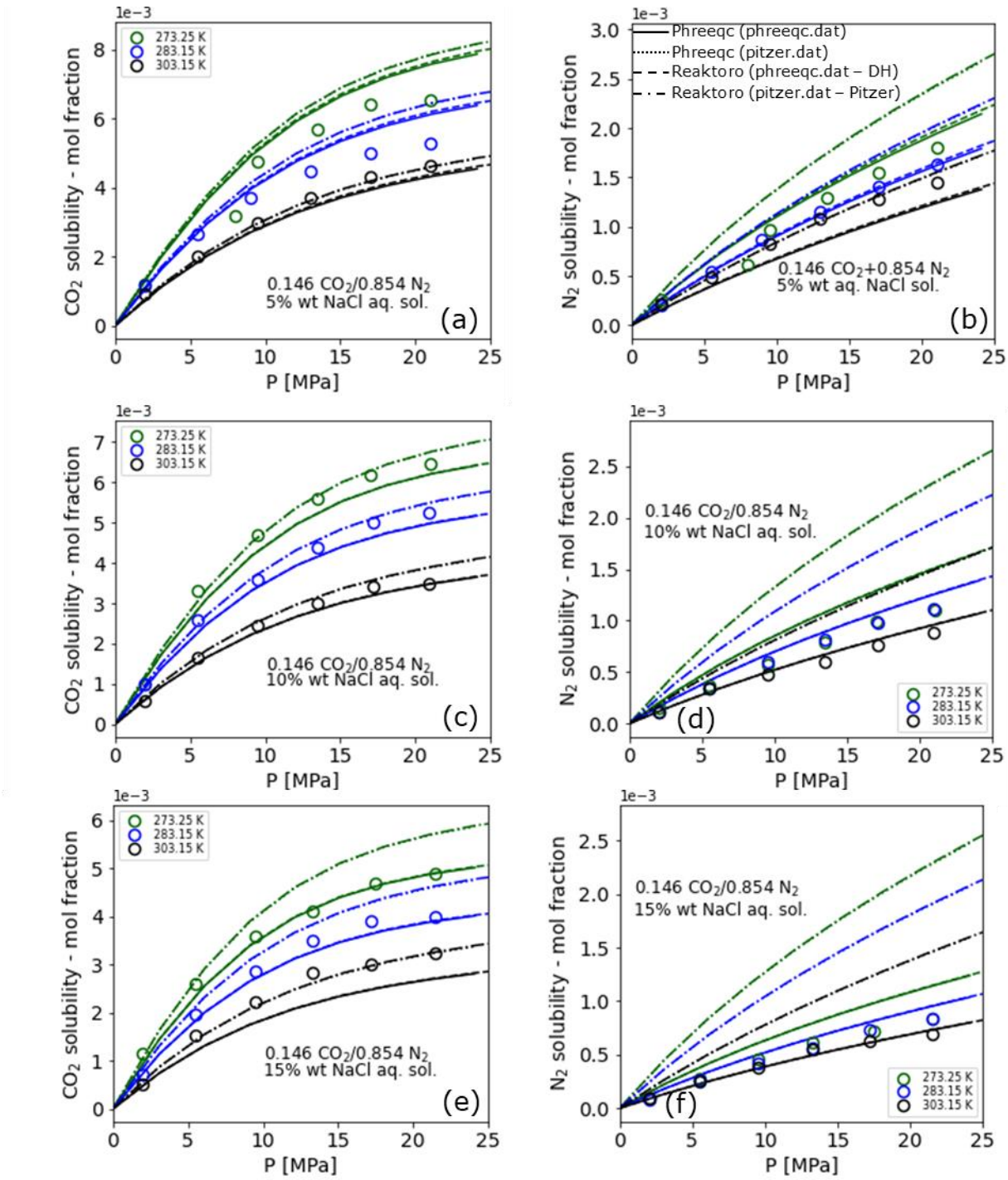

Figure 11. Co-solubility of CO_2 (panels a, c, e) and N_2 (panels b, d, f) in three different NaCl aqueous solutions, i.e., (a-b) 5 wt.%, (c-d) 10 wt. % and (e-f) 15 wt. % at different pressures and temperatures. The initial gas phase is a 0.146/0.854 CO_2/N_2 mixture.

The composition of the gas phase upon equilibration with the NaCl solutions predicted with both PHREEQC and Reaktoro is also compared with the experimentally inferred values. The performance of the models is displayed in Figure 12.

https://doi.org/10.26434/chemrxiv-2023-4hgnm **ORCID:** https://orcid.org/0000-0003-0475-323X Content not peer-reviewed by ChemRxiv. **License:** CC BY 4.0

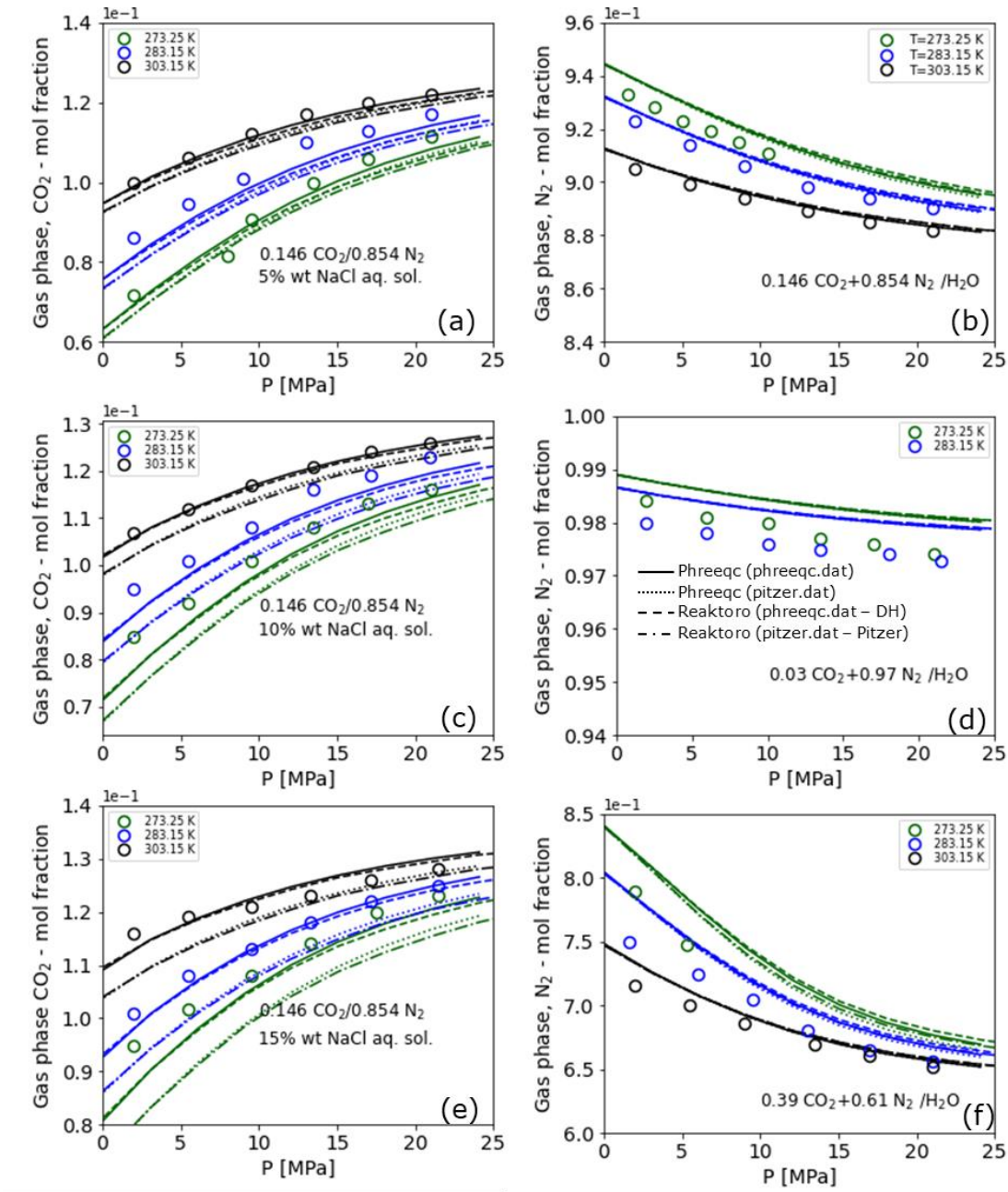

Figure 12. CO_2 (panels a, c, e) and N_2 (panels b, d, f) mol fractions in a CO_2/N_2 gas phase mixture upon equilibration with three different NaCl aqueous solutions, i.e., (a-b) 5 wt.%, (c-d) 10 wt. % and (e-f) 15 wt. % at different pressures and temperatures. Before equilibration, the gas phase contained 0.146/0.854 CO_2/N_2.

3.2.2 Carbon dioxide - Methane

Qin et al. [25] measured the distribution of methane and carbon dioxide between liquid and vapor in the H_2O, CO_2 and CH_4 ternary system up to 100ºC and 400 bar. Aqueous and gas phases were equilibrated between 8-36 h at the desired pressure and temperature. Gas and liquid samples were obtained upon equilibration. The volume of CH_4 emerging from the aqueous samples was measured and converted to moles using the ideal gas law. The dissolved CO_2 was completely converted to HCO_3^- and CO_3^{-2} by NaOH titrations, which were then quantified by coulometric titrations. Figure 13 shows the experimental and modelled solubility of CO_2 (panels a and c) and CH_4 (panels b and d) from the CO_2-CH_4 binary gas mixture in water represented as a function of the CO_2/CH_4 partial pressure upon equilibration.

https://doi.org/10.26434/chemrxiv-2023-4hgnm ORCID: https://orcid.org/0000-0003-0475-323X Content not peer-reviewed by ChemRxiv. License: CC BY 4.0

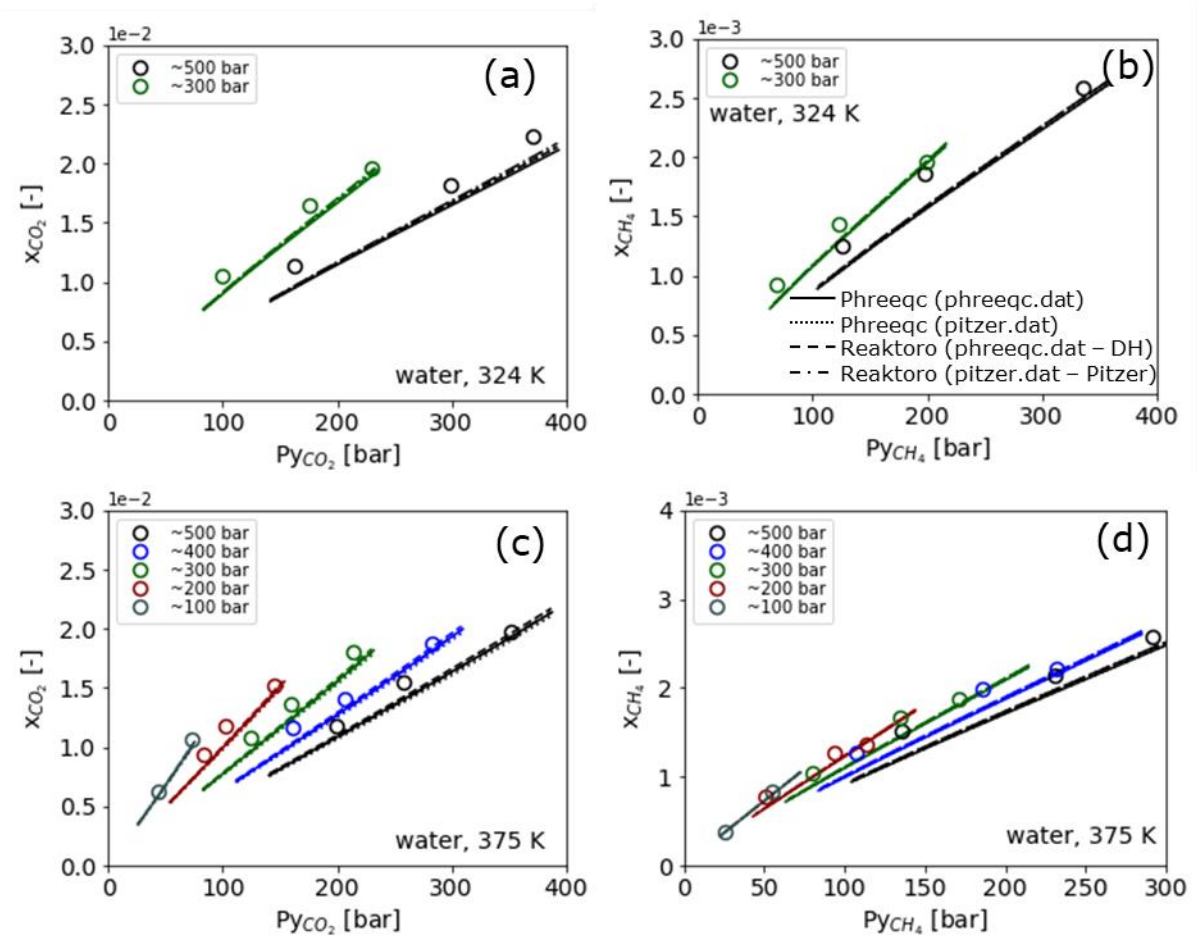

Figure 13. Co-solubility of CO_2 (panels a, c) and CH_4 (panels b, d) in water at different pressures and temperatures. Note that the x-axis represents the gas partial pressure of CO_2 and CH_4 upon equilibration. Markers represent the experimental data from [25].

3.3 Bubble point pressure and degassing potential of geothermal fluids

Models implemented in PHREEQC and Reaktoro are also used to predict the bubble point pressure, P_b, of different geothermal fluids. The phreeqc database was used in all cases since we previously showed that for some gases, the pitzer database did not account for the effect of salinity on the solubility. The predicted values were assessed against experimental evidence found in the literature. Compared to the previous solubility experiments considered, where the chemical composition of the system is relatively simple and carefully designed, the chemistry of the geothermal fluids is an amalgam of different ions and dissolved gases. The degassing point measured for these brines is thus a good way to test the performance of the models against fluid samples representative of natural conditions.

3.3.1 Merksplas-Beerse geothermal well

Vandenberghe et al. [26] obtained fluid samples from the Merksplas-Beerse geothermal well drilled into a karstic limestone section of the Dinantian reservoir. The reservoir fluid showed a high dissolved gas content. Chemical analyses were performed on several water samples obtained either at the gas separator outlet, from a corrosion test loop, or downhole samples. The water analyses on downhole samples and the gas composition of five gas samples, GLR, and measured bubble point pressure at 73.9ºC are shown in Table 1:

https://doi.org/10.26434/chemrxiv-2023-4hgnm ORCID: https://orcid.org/0000-0003-0475-323X Content not peer-reviewed by ChemRxiv. License: CC BY 4.0

Table 1. Gas and brine composition of downhole fluid samples from the Merksplas-Beerse geothermal well. Experimental data from [26]. S1 and S2 represent the water analysis on downhole samples and G1-G5 represent gas samples.

Ionic composition of brine samples in g/L														
	Na^+	K^+	Ca^{2+}	Mg^{2+}	Fe^{2+}	Fe^{3+}	Mn^{2+}	Ba^{2+}	Cl^-	SO_4^{2-}	SiO_3^-	HCO_3^-	NH_4^+	TDS
S1	33.5	1.79	10.1	0.97	0.0041	0.036	0.0045	0.003	70.9	0.652	0.046	0.35	0.17	137
S2	38.4	1.82	9.58	0.94	0	0.003	0.003	0.009	71.2	0.7	0.047	0.42	0.16	147

Gas composition [%], GLR [-] at standard conditions (1 atm and 273.15 K), bubble point pressure [bar] at 73.9ºC									
	Depth [m]	CO_2	CH_4	N_2	O_2	GLR	Mol. mass.	ρ [kg/m^3]	P_b [bar]
G1	1646	93.67	3.40	2.71	0.22	1.62	42.53	1.49	26.54
G2	1646	92.25	3.21	4.43	0.11	1.11	42.35	1.46	14.82
G3	1740	83.11	6.27	10.15	0.47	0.96	40.42	1.39	26.54
G4	1740	93.10	3.57	3.25	0.80	0.71	42.45	1.46	12.75
G5	1646	87.95	4.43	7.51	0.11	1.22	41.52	1.43	28.95

To calculate the bubble point pressure using PHREEQC, a solution and gas phase consistent with the specifications in Table 1 are defined and equilibrated at the experimental temperature and increasing pressure values. Since the composition of the two downhole samples is slightly different, we calculated the bubble point pressure considering both the composition of the "S1" and "S2" samples. The calculated bubble pressures are shown together with the experimental values in Figure 14. PHREEQC and Reaktoro lead to similar bubble point pressures and, except for two of the gas samples, which is in good agreement with the experimental results.

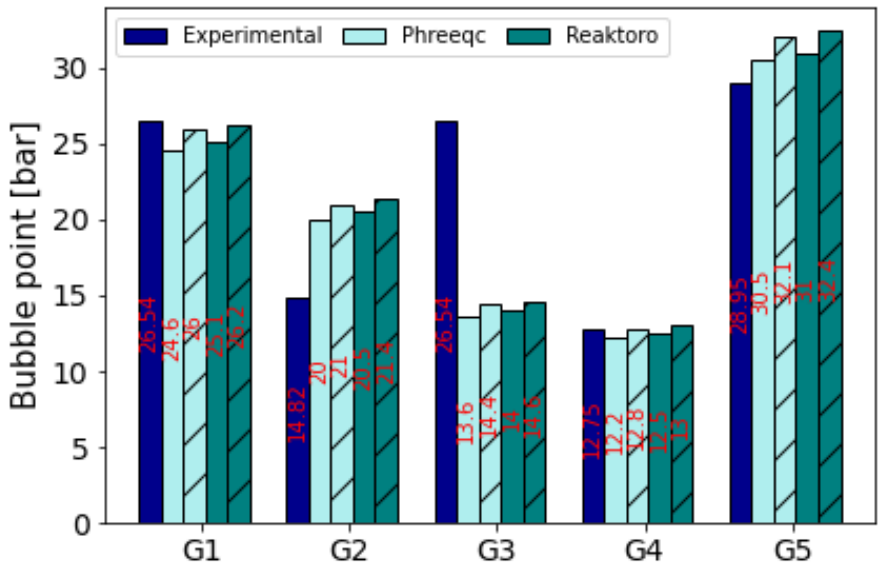

Figure 14. Comparison between the measured and calculated bubble point pressures. The bubble point was calculated for both brine samples. Solid colored and hatched bars correspond to the bubble point pressure considering "S1" and "S2" fluid samples, respectively. In all cases, the bubble point was calculated at 73.9ºC.

3.3.2 Soultz-sous-Forêts and Rittershoffen

Mouchot et al. [27] evaluated the first years of operation at two industrial geothermal plants in Soultz-sous-Forêts and Rittershoffen, both located in the French part of the Upper Rhine Grabben. These plants were commissioned in 2016. At Soultz-sous-Forêts, geothermal water is coming at the wellhead at 150ºC and 23 bar. In the Rittershoffen geothermal plant, brine is produced at 170ºC and 25 bar from a production well at 2700 m depth. The geothermal brines at the two sites are highly saline (i.e., ≈100 g/L), consisting mainly of Na^+, Ca^{+2} and Cl^- elements with a GLR of above 1 Nm^3/m^3. Due to the high

https://doi.org/10.26434/chemrxiv-2023-4hgnm ORCID: https://orcid.org/0000-0003-0475-323X Content not peer-reviewed by ChemRxiv. License: CC BY 4.0

amount of dissolved CO_2, the surface facilities at Soultz-sous- Forêts and Rittershoffen are operated at pressures of 23 and 25 bar, respectively, to avoid CO_2 degassing, steam flashing, and corrosion issues.

Table 2. Brine and gas composition at wellhead at Soultz-sous-Forêts (S1 and G1) and Rittershoffen (S2 and G2). Oxygen concentration is not mentioned but rather the remaining 1% represents oxygen, hydrogen, helium, Ar, H_2S, and ethane. For modelling purposes, the remaining 1% was assumed to be oxygen. Brine composition at Rittershoffen and Soultz-sous-Forêts taken from [28]. Gas compositions and GLR *from [27]*.

Ionic composition of brine samples in g/L										
	Na^+	K^+	Ca^{2+}	Mg^{2+}	Br-	$Fe2^+$	Cl^-	SO_4^{2-}	SiO_3^-	HCO_3^-
S1	28.14	3.19	7.22	0.13	0.271	0.025	58.55	0.157	0.063	0.167
S2	28.4	3.789	7.20	7.20	0.251	0.048	59.9	0.220	0.146	0.082

Gas composition [%], GLR [-] at standard conditions (1 atm and 273.15 K)						
	CO_2	CH_4	N_2	O_2	GLR	P_{op} [bar]
G1	91.0	2.0	7.0	-	1.03	23
G2	90	2.0	7.0	1.0	1.2	25

Although this study does not explicitly state the bubble point pressure, it specifies that the operating pressure in these two geothermal plants was selected so that the surface facilities are operated below the degassing point. Considering that all the information required for predicting the bubble point pressure is available, the calculated P_b is compared to the operating pressure in Figure 15. Both PHREEQC and Reaktoro predict a bubble point pressure slightly below the operating pressure. The calculated bubble point pressures are thus consistent with the fact that at 23 and 25 bar, respectively, the geothermal plants at Soultz-sous-Forêt and Rittershoffen are operated above the degassing pressure.

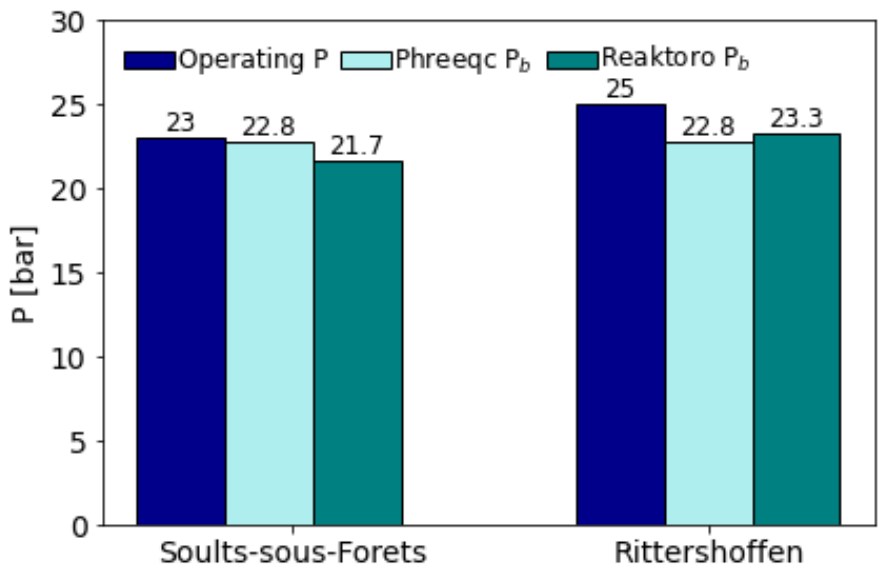

Figure 15. Bubble point pressure at Soultz-sous-Forêts and Rittershoffen estimated using Reaktoro and PHREEQC. The theoretical bubble point is assessed against the operating pressure at the two geothermal facilities. The operating pressure was chosen above the bubble point to avoid degassing. Operating pressures are taken from ref. [27]

3.3.3 Geothermal wells in the Netherlands

In the Netherlands, well monitoring and fluid sampling campaigns were carried out to assist in understanding the injectivity decline in several geothermal wells used for heating greenhouses. As part of these campaigns, ref. [29] gathered the chemical analyses at several sites from different geological formations in the Netherlands (e.g., Carboniferous, Rijswijk, Slochteren). In the mentioned report, the bubble point pressures at six sites were reported. Yet, among these six sites, only for three of them, the GLR ratio was included as well. Among the three sites that include both the bubble point pressure and

https://doi.org/10.26434/chemrxiv-2023-4hgnm ORCID: https://orcid.org/0000-0003-0475-323X Content not peer-reviewed by ChemRxiv. License: CC BY 4.0

the GLR, the gas composition is available only for one of them. Thus, only one experimental measurement (corresponding to site 3 in the mentioned report, Rijswijk formation) can be used for comparison to the bubble point pressure predicted by PHREEQC and Reaktoro. The composition of the fluids, i.e., gas and liquid, sampled at this site and the GLR are reported in Table 3. Note that the original reference does not clearly state whether the GLR is reported at standard conditions but for the calculations, it has been assumed so.

Table 3. Composition of the liquid and gas sampled at site 3 (denominated here as S1 and G1, respectively), Rijswijk formation. Experimental data from [29].

Ionic composition of brine samples in g/L				
	Na^+	Ca^{2+}	Cl^-	HCO_3^-
S1	34.4	3.64	67.71	0.164
Gas composition [%], GLR [-] assumed at standard conditions (1 atm and 273.15 K), bubble point pressure [bar] at 62.2ºC				
	CO_2	CH_4	GLR	P_b [bar]
G1	15	85	0.14	12.7

Considering the experimental data in Table 3, we described the chemical systems in both PHREEQC and Reaktoro. The bubble point pressures predicted with both software programs are shown in Figure 16 against the experimental value.

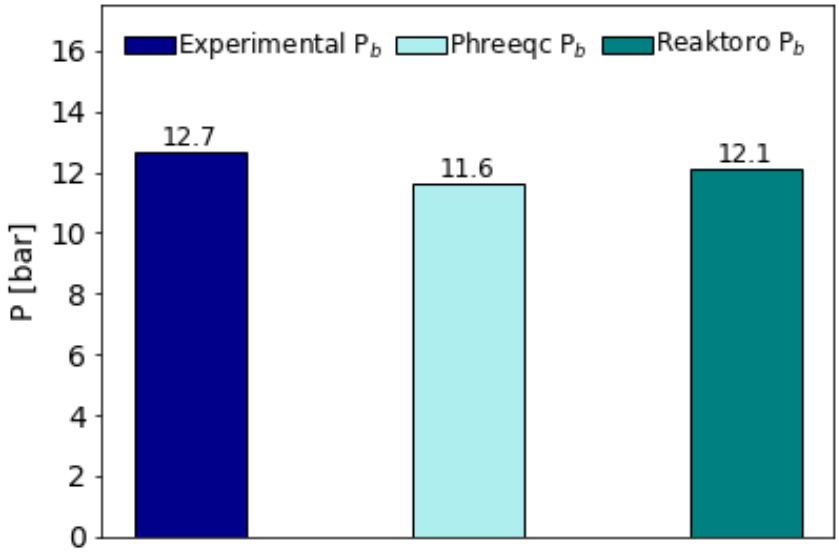

Figure 16. Comparison between the bubble point pressure measured at a sampling site at the Rijswijk formation and the theoretical values predicted with PHREEQC and Reaktoro. Experimental data from [29].

3.3.4 Bad Blumau

We further assessed PHREEQC and Reaktoro's performance for bubble point pressure calculations against the experimental data from Bad Blumau, Austria [30]. Originally, hydrocarbon exploration wells were drilled at this site, eventually used for geothermal and balneology purposes. A geothermal doublet, with water being produced at 110ºC, was established for the spa complex acclimatization. The gas-water ratio is very high, up to 9:1, with the gas phase consisting primarily of CO_2 (> 97%). Production logs showed that degassing started at a depth of 560 m. The bubble point pressure can thus be estimated from the hydrostatic pressure at the depth, where the onset of degassing was observed. Considering a brine density of approximately 1065 kg/m^3, the bubble point pressure is estimated at around 61 bar.

https://doi.org/10.26434/chemrxiv-2023-4hgnm ORCID: https://orcid.org/0000-0003-0475-323X Content not peer-reviewed by ChemRxiv. License: CC BY 4.0

The composition of the fluids at Bad Blumau (well 2) is given in Table 4. For the gas composition, CO_2 is mentioned as being the main component. Since the composition of the remaining 3% is not stated, nitrogen is assumed and considered for the calculations.

Table 4. Composition of the fluids from Bad Blumau 2. Experimental data from [30].

Ionic composition of brine samples in mg/L								
	Na^+	K^+	Ca^{2+}	Mg^{2+}	$Fe2^+$	Cl^-	SO_4^{2-}	HCO_3^-
S1	5799	129	31.7	6.4	0.025	3634	508	7834

Gas composition [%], GLR [-] at standard conditions (1 atm and 273.15 K), bubble point pressure (P_b) at 110 ºC				
	CO_2	N_2	GLR	P_{op} [bar]
G1	97.0	3.0	9.0	61

The experimental data from Table 4 was used to describe the gas-liquid equilibria at Bad Blumau. Considering these experimental conditions, the bubble point pressure was calculated with PHREEQC and Reaktoro. Figure 17 shows a comparison of the experimental bubble point pressures and the predicted values. The models' results are in good agreement with the experimental value, despite the uncertainty about the gas phase composition.

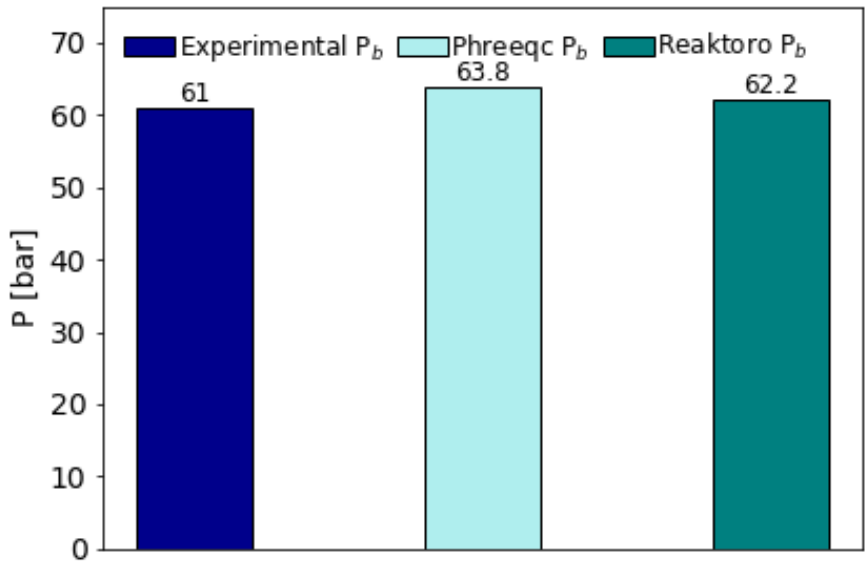

Figure 17. Comparison between the bubble point pressures at Bad Blumau and the values estimated with PHREEQC and Reaktoro. Experimental data from [30].

3.3.5 REFLECT project comparison

PHREEQC and Reaktoro were also validated against the experimental data gathered within the "REFLECT" project. The main objective of this European project was to prevent problems related to fluid chemistry. To improve the extent and performance of predictive modelling, the project focused on collecting and obtaining new and high-quality experimental data. Production and injection data was collected in a European geothermal fluid atlas. As part of this initiative, the geological, physical, and chemical information of samples from geothermal wells in different countries was gathered in a European geothermal fluid atlas. Despite the vast data included in the atlas, information on the bubble point pressure is available only for a very limited number of wells. Moreover, in some cases, the bubble point pressure is not accompanied by the additional information required for its theoretical prediction (e.g., the composition of the gas phase or the GLR is missing). Within the atlas, the complete information for bubble point pressure calculation and comparison is available only for 5 wells (i.e.,

https://doi.org/10.26434/chemrxiv-2023-4hgnm ORCID: https://orcid.org/0000-0003-0475-323X Content not peer-reviewed by ChemRxiv. License: CC BY 4.0

three from France and two from the Netherlands). The fluid chemistry data for these wells is gathered in Table 5.

Table 5. Properties of fluids sampled from three geothermal production wells in France and the Netherlands. Experimental data from [31]. Samples S1-S3 and G1-G3 correspond to fluids (liquid and gas, respectively) from wells in France, whereas S4-S5 and G4-G5 correspond to samples from the Netherlands.

Ionic composition of brine samples in g/L											
	Well ID	Na^+	K^+	Ca^{2+}	Mg^{2+}	Fe^{3+} /Fe^{2+}	Sr^{2+}	Cl^-	SO_4^{2-}	SiO_3^-	HCO_3^-
S1	W-Fr-066-FS001	3.83	0.06	1.84	0.15	0.003	0.03	8.89	0.66	0.019	0.585
S2	W-Fr-077-FS001	4.1	0.07	0.51	0.1	-	0.02	7.0	0.79	0.019	0.446
S3	W-Fr-079-FS002	7.9	0.14	1.9	0.31	0.008	0.04	16	1.1	-	0.440
S4	W-NL-001	43	0.43	5.9	0.9	0.076	0.35	78	0.33	-	-
S5	W-NL-009	34	0.97	3.9	1.0	0.033	-	81	0.09	0.008	0.170

Gas composition [%], GLR [-] at standard conditions (1 atm and 273.15 K), bubble point pressure [bar]									
	CO_2	CH_4	N_2	O_2	H_2	H_2S	GLR	T [ºC]	P_b [bar]
G1	86.17	8.9	4.22	-	0.19	-	0.7	71	9
G2	28.44	31.06	34.47	-	-	-	0.28	73.7	5.2-5.9
G3	75.15	3.37	18.34	2.87	-	-	0.16	72	5.5
G4	3.2	89.7	4.3	-	-	-	1.07	86	48.3
G5	3.37	77.86	1.52	-	-	-	1.24	76	91

To calculate the bubble point pressure for the fluid systems described in Table 5, the solution and gas-phase compositions were defined in PHREEQC and Reaktoro. Some of the compositions for the aqueous and gas fluids show charge and mass imbalance, respectively. To ensure solution electroneutrality, the charge was balanced with Cl^-. To keep the mass balance, the gas concentrations found in the atlas were normalized. Moreover, it is uncertain whether the GLR was normalized to standard conditions (e.g., 1 atm and 273.15 K) or whether it is reported at the sampling temperature. Thus, the bubble point pressure is estimated considering both cases. The comparison between PHREEQC and Reaktoro and the experimental data is shown in Figure 18. The consistency between the models and the experimental data is fair only for one sample from the Netherlands and two from France. Moreover, the predicted bubble point pressure is impacted considerably by the conditions at which the GLR is reported. Considering that the GLR is reported at the production temperature leads to a bubble point pressure in better agreement with the experimental value.

https://doi.org/10.26434/chemrxiv-2023-4hgnm **ORCID:** https://orcid.org/0000-0003-0475-323X Content not peer-reviewed by ChemRxiv. **License:** CC BY 4.0

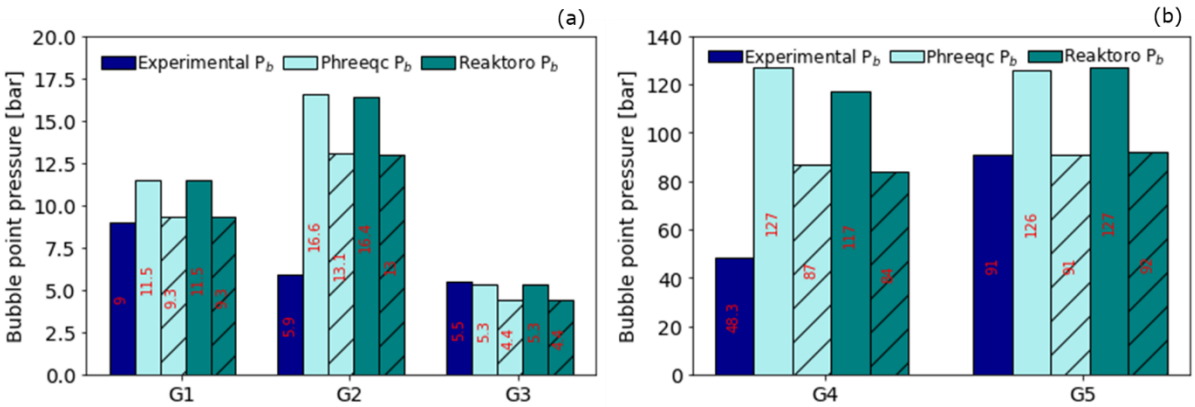

Figure 18. Comparison between the bubble point pressure measured on fluid samples from (a) wells in France and (b) wells in the Netherlands and degassing pressures predicted with PHREEQC and Reaktoro. Solid bars were calculated considering that the GLR was reported at standard conditions (i.e., 1 atm 273.15 K), whereas hatched bars were calculated considering that the GLR was reported at the production temperature conditions (values included in Table 5).

3.3.6 Margretheholm geothermal plant

PHREEQC and Reaktoro were also used to predict the bubble point pressure at the Margretheholm geothermal plant in Copenhagen. At this facility, highly saline brine (19% wt) at 72ºC is produced to provide 14 MW heat for district heating purposes [32]. When starting up the plant, it was found that the bubble point pressure was higher than it had been previously estimated from water/gas samples. The production wellhead pressure was therefore increased to 15 bar. The bubble point pressure was then estimated at around 20 bar [32]; yet no information on the fluid composition, besides the overall salinity, is provided. Thus, to determine the bubble point pressure with PHREEQC and Reaktoro, the composition at Margretheholm is taken from ref [33]. A slightly different composition is reported in ref [34]. The fluid composition considered in our calculations is included in Table 6.

Table 6. Composition of the fluids at Margretheholm. [33].

Ionic composition of brine samples in g/L												
	Na^+	K^+	Ca^{2+}	Mg^{2+}	Br-	Cl^-	SO_4^{2-}	Mn^{+2}	HCO_3^-	NH_4^+	Sr^{+2}	SiO_3^-
S1	53.97	0.63	20.5	2.93	0.82	128.8	0.261	0.006	0.029	0.021	0.86	0.006

Gas composition [%], GLR [-] at standard conditions (1 atm and 273.15 K), bubble point pressure at 72ºC						
	CO_2	CH_4	N_2	O_2	GLR	P_b [bar]
G1	2.4	5.2	93.9	0.66	0.15	20

The evolution of the gas volume per unit volume of solution for the Margretheholm fluid is shown in Figure 19. The gas-liquid equilibration was calculated under different scenarios. The black line corresponds to the gas-liquid volume ratio at different pressures considering the fluid composition described in Table 6; this leads to a degassing pressure of approximately 50 bar, considerably above the bubble point pressure estimated during the operation of the geothermal facility. The calculated bubble point pressure decreases considerably, i.e., to approximately 36 bar when considering that the GLR is not extrapolated at standard temperature but measured at the production temperature (blue line). Moreover, describing the fluid composition in terms of NaCl salinity only, further decreases the bubble point pressure up to approximately 28 bar. Taking into account the exact fluid composition plays a great effect on the predicted bubble point pressure. Moreover, all scenarios considered predict a much higher bubble point pressure than what was determined operationally as degassing pressure. Yet, at 20 bar, the pressure at which degassing was estimated to take place during operation, simulations show that the volume of gas is less than 2% compared to that of the solution. Generally, standard centrifugal pumps can be used for entrained gases up to 4% by volume. It is possible that operationally, even though

https://doi.org/10.26434/chemrxiv-2023-4hgnm ORCID: https://orcid.org/0000-0003-0475-323X Content not peer-reviewed by ChemRxiv. License: CC BY 4.0

degassing might have occurred at higher pressures, the amount of gas is not considerable enough to impair operation. Thus, the pressure that leads to relevant degassing during operation, it is not necessarily a "true" bubble point pressure, which could eventually be much higher.

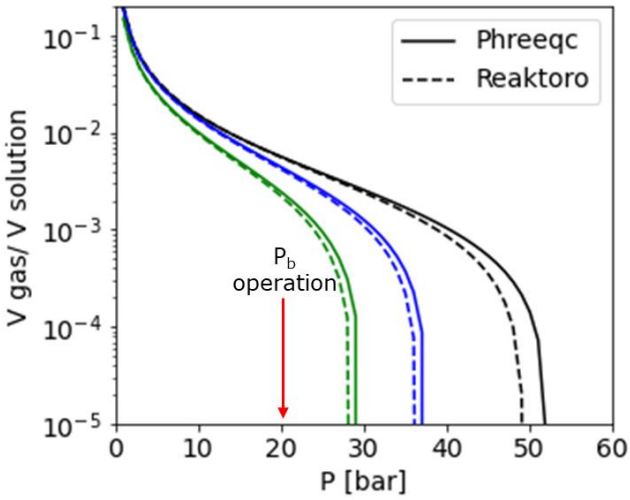

Figure 19. Ratio of the gas and liquid phase volumes at different pressures. The line colors correspond to three different simulation scenarios: brine composition in Table *6* and GLR considered at standard conditions (black lines), brine composition in Table *6* and GLR assumed at the production brine temperature (72 ºC), brine composition defined simply as 19% NaCl salinity and GLR considered at standard conditions (green lines). The red arrow represents the bubble point pressure that was estimated during the operation of the geothermal facility.

3.3.7 Malm Aquifer

Next, we used the bubble point pressures reported in the work of Baumann [12] to assess the performance of PHREEQC and Reaktoro. In the mentioned reference, the author compares the bubble point pressures estimated with PHREEQC against experimental values on samples taken from the Malm Aquifer in the Bavarian Molasse Basin. The composition of the geothermal fluids is included in Table 7.

Table 7. Ionic composition of the fluids. Besides the gases included here, the original reference reports also a lower content of other gases such as ethane, hydrogen, which add up to 1.2% (mol). These minor gases have not been included in the simulation.

Ionic composition of brine samples in mg/L									
	Na^+	K^+	Ca^{2+}	Mg^{2+}	S^{-2}	Cl^-	SO_4^{2-}	F^-	HCO_3^-
S1	112	16.8	13.2	4.98	10.7	122	6.0	4.19	0.029
S2	115	17.5	27.9	4.5	30.5	110	11	-	222

Gas composition [%], GLR [-] at standard conditions (1 atm and 273.15 K), bubble point pressure at 145 ºC						
	CO_2	CH_4	N_2	H_2S	GLR	P_b [bar]
G1	43	32	19.3	5.1	0.136	4.1
G2	61	25.1	13.1	-	0.148	3.9

Generally, the calculated bubble point pressures with both Reaktoro and PHREEQC are very similar and in good agreement with the experimental observations (Figure 20). The degassing pressures calculated in the work of Baumann using PHREEQC are slightly higher than our predictions. The differences could most likely be attributed to differences in the model implementation. For instance, in PHREEQC, Baumann defined CH_4, C_2H_6, and N_2 within an "EQUILIBRIUM_PHASES" block, whereas the CO_2 and H_2S were added as a "GAS_PHASE". In our implementation, only a "GAS_PHASE" of fixed pressure containing all gas components was defined. Further discrepancies might have arisen from the fact that we did not define the concentration of lower concentration gases (e.g., ethane with a molar concentration below 1%). To close the material balance for the gas phase and

https://doi.org/10.26434/chemrxiv-2023-4hgnm ORCID: https://orcid.org/0000-0003-0475-323X Content not peer-reviewed by ChemRxiv. License: CC BY 4.0

also account for the lighter gas fractions, we included a slightly higher concentration of methane (i.e., as reported in Table 7).

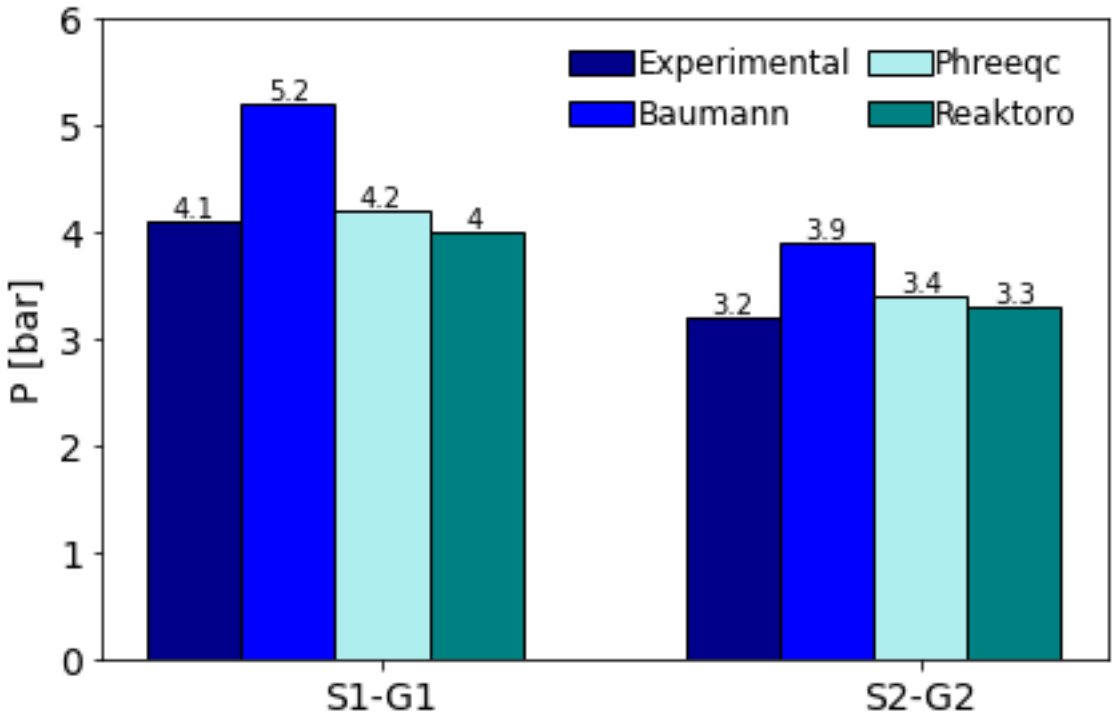

Figure 20. Comparison between the bubble point pressures calculated using PHREEQC and Reaktoro with the experimental and calculated bubble point pressures in ref. [12]. The value labeled as "Baumann" corresponds to the bubble point pressure calculated by Baumann [12] using PHREEQC.

3.3.8 Model vs model comparison

Lastly, our bubble point pressure calculations using PHREEQC and Reaktoro are also compared against those estimated by Köhl et al. [16] using PHREEQC. Note that this represents a model versus model comparison, as Köhl et al. [16] did not validate their calculations against any experimental data.

The composition of the fluids (gas and brine) is included in Table 8. Note that the composition of major ions, e.g., Na^+ and Cl^- was not stated explicitly but given in a lumped way. Thus, the composition of Na^+ and Cl^- was recalculated from the Ca^{+2}, Mg^{+2}, and HCO_3^- and considering the overall solution electroneutrality. Monovalent cations other than Na^+ were ignored. Sulfur-containing components were also mentioned in the original paper. Yet, since the distribution of these components is not clearly stated, the brine composition was characterized only in terms of the major ions in Table 8.

https://doi.org/10.26434/chemrxiv-2023-4hgnm **ORCID:** https://orcid.org/0000-0003-0475-323X Content not peer-reviewed by ChemRxiv. **License:** CC BY 4.0

Table 8. Composition of fluid samples from the Bavarian Molasse Basin. Experimental data based on ref. [16].

Ionic composition of brine samples in mg/L					
	Na^+	Ca^{2+}	Mg^{2+}	Cl^-	$CO_2(aq) + HCO_3^-$
S1	175.95	43.6	6.0	186.37	503.92
S2	144.21	23.2	2.88	153	323.76
S3	110.17	16.8	2.16	57.8	469
S4	138.69	28.4	4.32	102.6	414.52
S5	140.53	34	4.32	144.13	338.71

Gas composition [%], GLR [-] at standard conditions (1 atm and 273.15 K)					
	CO_2	CH_4	N_2	GLR	T
G1	0.19	0.29	0.52	0.23	55
G2	0.11	0.3	0.59	0.08	32
G3	0.17	0.37	0.46	0.09	52
G4	0.2	0.34	0.46	0.04	69
G5	0.12	0.46	0.42	0.05	57

Considering the fluid composition in Table 8, the bubble point pressures that we calculated with PHREEQC and Reaktoro are compared with the degassing pressures calculated by Köhl et al. [16]. It is important to note that both in ref. [16] and this paper, the bubble point pressure corresponds to the pressure that leads to a gas volume in the order of 1×10^{-5} L/L of solution. Generally, our calculations are in fair agreement with those from Köhl et al. [16]. Differences in the defined brine composition could justify some of the greater discrepancies observed for the "S2-G2" and "S3-G3" systems.

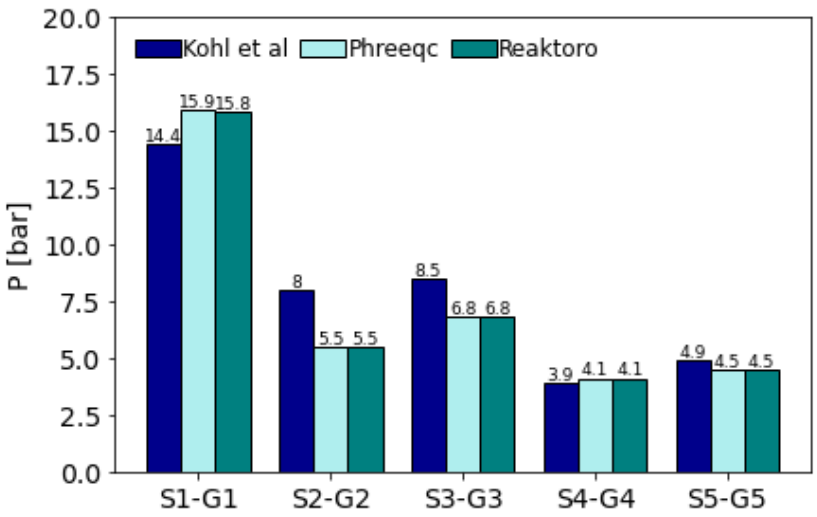

Figure 21. Comparison of the bubble point pressures predicted with PHREEQC and Reaktoro to those calculated by Köhl et al. [16].

4 Discussion

The solubility of gases in water and aqueous solutions is relevant to uncounted industrial processes (e.g., flue gas conditioning, CO_2 capture and transportation, underground fluid extraction/injection). The design and operation of such processes can be optimized via models that can accurately simulate the partitioning of these gases between an aqueous and gaseous phase. Our results show that the models implemented in PHREEQC and Reaktoro predict very well the solubility of individual gases such as CH_4, N_2, CO_2, H_2S, O_2, and H_2 in water at a high range of temperature and pressure conditions with both phreeqc and pitzer databases. Yet, for higher ionic strength systems, where non-idealities prevail, the performance of the models is heavily impacted by the selected thermodynamic database. While "phreeqc.dat" reflects correctly the decreasing CH_4, N_2, H_2, and O_2 solubility in electrolyte solutions of

https://doi.org/10.26434/chemrxiv-2023-4hgnm ORCID: https://orcid.org/0000-0003-0475-323X Content not peer-reviewed by ChemRxiv. License: CC BY 4.0

increasing ionic strength (Figures 2, 3, 67, and 77, respectively), "pitzer.dat" does not account for the effect of salinity on the solubility of these individual gases. The opposite is observed for the CO_2 and H_2S gas systems (Figures 4 and 5, respectively), whose solubility in brines is more accurately described by the pitzer database compared to phreeqc.dat. The default pitzer database distributed with PHREEQC contains interaction parameters between H_2S with Cl^-, Na^+, and SO_4^{-2} and between CO_2 with HSO_4^-, SO_4^{-2}, Na^+, Mg^{+2}, and K^+, which eventually improves its performance compared to phreeqc.dat for CO_2 and H_2S systems. These interactions are not defined for the other gases tested in this work. This pitfall can be handled by editing the database and defining interaction parameters between the different gases and ionic species as previously suggested in [11].

The results obtained with PHREEQC and Reaktoro are generally equivalent, which is essentially due to the analogous implementation with respect to the used database and the thermodynamic models for describing the aqueous and gaseous phase. Yet, with phreeqc.dat, some inconsistencies have been observed between the two software programs; while neither PHREEQC nor Reaktoro predict particularly well the solubility of methane in Na_2CO_3 solutions, Reaktoro outperforms PHREEQC at predicting the solubility of methane in $MgSO_4$ solutions (see Figure 1 panels, e and g, respectively).

Solubility measurements from multicomponent gas systems are still relatively scarce. The few experimental datasets involving binary gas systems found and gathered in this work show that PHREEQC and Reaktoro quantify reasonably well the co-solubility of CO_2, N_2, and CH_4 from either CO_2-N_2 or CH_4-CO_2 binary gas mixtures, providing a good description of the equilibrium compositions in the aqueous and gaseous phase. To test PHREEQC and Reaktoro under conditions that are more representative of natural systems, these were compared against the limited bubble point pressure measurements reported in the literature. In this case, the aqueous solutions were not simply synthetic brines prepared in a laboratory, but samples obtained from geothermal wells. Considering the compositional assortment of natural waters, the agreement between the predicted and measured bubble point pressures varied from sample to sample; in some cases, the consistency between the predicted and measured dataset is fairly good (e.g., Figures 15 to 17), whereas in some other cases, a greater discrepancy is observed. There are several factors, stemming either from the experimental protocols or model limitations, that may explain the discrepancies. Firstly, the gas samples at many sites consist of a mixture of many different components. Yet, we showed that no database can handle all gas types with the same accuracy. Thus, the two databases tested may not perfectly describe the fluid mixtures considered. Secondly, the measured bubble point pressure is also impacted by how it was determined. Different sampling, fluid handling, and measurement techniques may lead to different results. Moreover, the definition of the bubble point pressure may also drive to contrasting modelled and measured values. Theoretically, the bubble point pressure is the pressure at which the first bubble of gas appears within a liquid. However, experimentally, depending on the technique used, the onset of degassing may not be recorded with the same precision. In many cases, the bubble point pressure is determined using a visual criterion, whereas within the models, we always reported the P_b as the pressure at which the volume of gas is above 1×10^{-5} L/ L of solution. Lastly, a mismatch can also be introduced simply because the modelled system is not representative of the real experimental conditions. As mentioned in the results section, some of the experimental datasets either do not clearly state which conditions the GLR is given at or contain flaws in the reported solution and gas composition, i.e., charge and mass imbalance, respectively. To deal with these obstacles, in the models, we ensured electroneutrality by adding/removing chloride and by normalizing gas compositions. Yet, the fidelity of the models and their predictability can only be achieved by a proper chemical (experimental) characterization of the fluids.

Compared to other publications that have calculated theoretical degassing pressures with PHREEQC, the models implemented in this work yielded similar but not equal values (Figures 20 and 21). We postulate that these differences are either because of slight differences in the implementation or defined fluid and gas composition. Yet, note that in one of these publications , i.e., [16], the modelled values

https://doi.org/10.26434/chemrxiv-2023-4hgnm ORCID: https://orcid.org/0000-0003-0475-323X Content not peer-reviewed by ChemRxiv. License: CC BY 4.0

were not tested against any experimental measurements. Besides PHREEQC and Reaktoro, different alternatives for modelling the solubility of gases in water and aqueous solutions have been proposed and discussed in the literature, e.g., [19], [21], [22], [24], [35]. These papers often introduce an in-house implementation of a specific thermodynamic model, whose performance is usually shown for a specific gas. Yet compared to PHREEQC and Reaktoro, these in-house developed codes are often not accessible by the wider community.

While we encourage the use of free/open-source software programs such as PHREEQC and Reaktoro in aiding the process design of, e.g., geothermal and CCS application, it is important that the users are familiar with the existing databases and their limitations. Any model predictions should be questioned if a prior validation against reliable experimental data has not been performed. Lastly, both phreeqc.dat and pitzer.dat include a double definition for some of the gases available, i.e., redox coupled and uncoupled. In the first case, the dissolved gas may undergo further redox reactions, leading to other aqueous species. For instance, in the redox coupled scenario, the conversion of $CH_{4,aq}$ and $N_{2,aq}$ to other inorganic carbon species and ammonium, respectively, maintains the brine undersaturated with respect to aqueous methane and nitrogen, allowing further gas dissolution. The difference between the two definitions becomes more relevant when complex aqueous compositions are defined, which could lead to a high redox potential and eventually cause certain aqueous species to reduce or oxidize. For the specific applications we addressed in this work, redox reactions are not deemed relevant, hence the redox uncoupled implementation used in this work.

5 Conclusions

Chemical models implemented in PHREEQC and Reaktoro were validated against a wide range of solubility measurements of individual and binary gas systems in water and aqueous solutions containing high electrolyte concentrations at a wide range of temperature and pressure conditions. When using the same database and thermodynamic models for describing the aqueous and gaseous phases, PHREEQC and Reaktoro yield analogous results. The performance of the models for describing the equilibria between multicomponent gas systems and complex brines was assessed against the bubble point pressures reported at several geothermal sites. The models satisfactorily predict the degassing pressure of different geothermal fluids but are overall susceptible to the amount of information available (or the lack of it) in the experimental sampling reports. From the two databases tested in this work, i.e., phreeqc.dat and pitzer.dat, the former was generally more versatile for the wide range of simulated conditions. The overall good agreement between the models and the experimental data shows that PHREEQC and Reaktoro are valuable tools that can be used in the early design of geothermal facilities, conditioning of gas and liquid streams (e.g., CO_2, H_2, produced water) or any other systems involving interactions between water/brine, gases, and minerals.

Acknowledgement

The authors would like to thank language secretary Susanne Tolstrup, Technical Safety Department, in Ramboll Energy, Energy Transition for proofreading this manuscript. The present work is partially supported by the Innovation Fund Denmark partnership “INNO-CCUS” and the work-package “CarbonAdapt”. The INNO-CCUS Partnership is established as a mean to secure a significant contribution to achieve the Danish government’s climate goals on CO_2 reduction, through CCUS solutions. This work is part of developing understanding and testing applicability of models for predicting solubility of gases in saline aqueous solutions.

https://doi.org/10.26434/chemrxiv-2023-4hgnm **ORCID:** https://orcid.org/0000-0003-0475-323X Content not peer-reviewed by ChemRxiv. **License:** CC BY 4.0

References

[1] T. Akin, A. Guney, and H. Kargi, "MODELING OF CALCITE SCALING AND ESTIMATION OF GAS BREAKOUT DEPTH IN A GEOTHERMAL WELL BY USING PHREEQC," in *Fortieth Workshop on Geothermal Reservoir Engineering*, Stanford University, Stanford, California, January 26-28, 2015.

[2] M. El Haj Assad, E. Bani-Hani, and M. Khalil, "Performance of geothermal power plants (single, dual, and binary) to compensate for LHC-CERN power consumption: comparative study," *Geotherm. Energy*, vol. 5, no. 1, p. 17, Sep. 2017, doi: 10.1186/s40517-017-0074-z.

[3] S. Frick *et al.*, "Geochemical and Process Engineering Challenges for Geothermal Power Generation," *Chem. Ing. Tech.*, vol. 83, no. 12, pp. 2093–2104, 2011, doi: 10.1002/cite.201100131.

[4] T. J. Wolery, "EQ3NR, a computer program for geochemical aqueous speciation-solubility calculations: Theoretical manual, user`s guide, and related documentation (Version 7.0); Part 3," Lawrence Livermore National Lab. (LLNL), Livermore, CA (United States), UCRL-MA-110662-Pt.3, Sep. 1992. doi: 10.2172/138643.

[5] J. P. Gustafsson, "Visual MINTEQ ver. 3.1." KTH Royal Institute of Technology, 2013. [Online]. Available: https://vminteq.lwr.kth.se/

[6] D. Parkhurst and C. A. J. Appelo, "Description of input and examples for PHREEQC version 3: a computer program for speciation, batch-reaction, one-dimensional transport, and inverse geochemical calculations," 6-A43, 2013. Accessed: Dec. 16, 2022. [Online]. Available: https://pubs.er.usgs.gov/publication/tm6A43

[7] A. M. M. Leal, "Reaktoro: An open-source unified framework for modeling chemically reactive systems. https://reaktoro.org." 2015.

[8] A. V. García, K. Thomsen, and E. H. Stenby, "Prediction of mineral scale formation in geothermal and oilfield operations using the extended UNIQUAC model: Part I. Sulfate scaling minerals," *Geothermics*, vol. 34, no. 1, pp. 61–97, Feb. 2005, doi: 10.1016/j.geothermics.2004.11.002.

[9] I. Søreide and C. H. Whitson, "Peng-Robinson predictions for hydrocarbons, CO2, N2, and H2 S with pure water and NaCI brine," *Fluid Phase Equilibria*, vol. 77, pp. 217–240, Sep. 1992, doi: 10.1016/0378-3812(92)85105-H.

[10] T. Hörbrand, T. Baumann, and H. C. Moog, "Validation of hydrogeochemical databases for problems in deep geothermal energy," *Geotherm. Energy*, vol. 6, no. 1, p. 20, Oct. 2018, doi: 10.1186/s40517-018-0106-3.

[11] K. Dideriksen, H. Holmslykke, and C. Kjøller, "PERFORM. WP2: Predict and validate," GEUS, PERFORM-D2.1, 2021.

[12] T. Baumann, "Validation of Hydrochemical Analyses and Gas Concentrations of Deep Geothermal Aquifers," in *41st Workshop on Geothermal Reservoir Engineering*, Stanford University, Stanford, California, February 22-24, 2016.

[13] C. A. J. Appelo, D. L. Parkhurst, and V. E. A. Post, "Equations for calculating hydrogeochemical reactions of minerals and gases such as CO2 at high pressures and temperatures," *Geochim. Cosmochim. Acta*, vol. 125, pp. 49–67, Jan. 2014, doi: 10.1016/j.gca.2013.10.003.

[14] C. A. J. Appelo, "Principles, caveats and improvements in databases for calculating hydrogeochemical reactions in saline waters from 0 to 200°C and 1 to 1000atm," *Appl. Geochem.*, vol. 55, pp. 62–71, Apr. 2015, doi: 10.1016/j.apgeochem.2014.11.007.

[15] C. A. J. Appelo and D. Postma, *Geochemistry, Groundwater and Pollution*. CRC Press, 2004.

[16] B. Köhl, M. Elsner, and T. Baumann, "Hydrochemical and operational parameters driving carbonate scale kinetics at geothermal facilities in the Bavarian Molasse Basin," *Geotherm. Energy*, vol. 8, no. 1, p. 26, Oct. 2020, doi: 10.1186/s40517-020-00180-x.

[17] R. K. Stoessell and P. A. Byrne, "Salting-out of methane in single-salt solutions at 25°C and below 800 psia," *Geochim. Cosmochim. Acta*, vol. 46, no. 8, pp. 1327–1332, Aug. 1982, doi: 10.1016/0016-7037(82)90268-X.

https://doi.org/10.26434/chemrxiv-2023-4hgnm **ORCID:** https://orcid.org/0000-0003-0475-323X Content not peer-reviewed by ChemRxiv. **License:** CC BY 4.0

[18] T. D. O'Sullivan and N. O. Smith, "Solubility and partial molar volume of nitrogen and methane in water and in aqueous sodium chloride from 50 to 125.deg. and 100 to 600 atm," *J. Phys. Chem.*, vol. 74, no. 7, pp. 1460–1466, Apr. 1970, doi: 10.1021/j100702a012.
[19] J. Xia, Á. Pérez-Salado Kamps, B. Rumpf, and G. Maurer, "Solubility of Hydrogen Sulfide in Aqueous Solutions of the Single Salts Sodium Sulfate, Ammonium Sulfate, Sodium Chloride, and Ammonium Chloride at Temperatures from 313 to 393 K and Total Pressures up to 10 MPa," *Ind. Eng. Chem. Res.*, vol. 39, no. 4, pp. 1064–1073, Apr. 2000, doi: 10.1021/ie990416p.
[20] W. Yan, S. Huang, and E. H. Stenby, "Measurement and modeling of CO2 solubility in NaCl brine and CO2–saturated NaCl brine density," *Int. J. Greenh. Gas Control*, vol. 5, no. 6, pp. 1460–1477, Nov. 2011, doi: 10.1016/j.ijggc.2011.08.004.
[21] S. Chabab, P. Théveneau, C. Coquelet, J. Corvisier, and P. Paricaud, "Measurements and predictive models of high-pressure H2 solubility in brine (H2O+NaCl) for underground hydrogen storage application," *Int. J. Hydrog. Energy*, vol. 45, no. 56, pp. 32206–32220, Nov. 2020, doi: 10.1016/j.ijhydene.2020.08.192.
[22] S. Chabab *et al.*, "Measurements and Modeling of High-Pressure O2 and CO2 Solubility in Brine (H2O + NaCl) between 303 and 373 K and Pressures up to 36 MPa," *J. Chem. Eng. Data*, vol. 66, no. 1, pp. 609–620, Jan. 2021, doi: 10.1021/acs.jced.0c00799.
[23] Y. Liu, M. Hou, H. Ning, D. Yang, G. Yang, and B. Han, "Phase Equilibria of CO2 + N2 + H2O and N2 + CO2 + H2O + NaCl + KCl + CaCl2 Systems at Different Temperatures and Pressures," *J. Chem. Eng. Data*, vol. 57, no. 7, pp. 1928–1932, Jul. 2012, doi: 10.1021/je3000958.
[24] A. Hassanpouryouzband *et al.*, "Solubility of Flue Gas or Carbon Dioxide-Nitrogen Gas Mixtures in Water and Aqueous Solutions of Salts: Experimental Measurement and Thermodynamic Modeling," *Ind. Eng. Chem. Res.*, vol. 58, no. 8, pp. 3377–3394, Feb. 2019, doi: 10.1021/acs.iecr.8b04352.
[25] J. Qin, R. J. Rosenbauer, and Z. Duan, "Experimental Measurements of Vapor–Liquid Equilibria of the H2O + CO2 + CH4 Ternary System," *J. Chem. Eng. Data*, vol. 53, no. 6, pp. 1246–1249, Jun. 2008, doi: 10.1021/je700473e.
[26] N. Vandenberghe, M. Dusar, P. Boonen, L. S. Fan, R. Voets, and J. Bouckaert, "The Merksplas-Beerse geothermal well (17W265) and the Dinantian reservoir," *Geol. Belg.*, Oct. 2001, doi: 10.20341/gb.2014.037.
[27] J. Mouchot *et al.*, "First Year of Operation from EGS Geothermal Plants in Alsace, France: Scaling Issues," in *43rd workshop on geothermal reservoir engineering*, 2018.
[28] B. Sanjuan, R. Millot, Ch. Innocent, Ch. Dezayes, J. Scheiber, and M. Brach, "Major geochemical characteristics of geothermal brines from the Upper Rhine Graben granitic basement with constraints on temperature and circulation," *Chem. Geol.*, vol. 428, pp. 27–47, Jun. 2016, doi: 10.1016/j.chemgeo.2016.02.021.
[29] GPC, KWR, "Report assessment of injectivity problems in geothermal greenhouse heating wells," Feb. 2015.
[30] J. Goldbrunner, "Bad Blumau (Styria, Austria). The success story of combined used of geothermal energy.," *GHC Bull.*, Jun. 2005.
[31] Helmholtz Centre Potsdam - GFZ, "European Fluid Atlas https://www.reflect-h2020.eu/efa/." 2020.
[32] A. Mahler and J. Magtengaard, "Country update report for Denmark," in *Proceedings World Geothermal Congress 2010*, Bali, Indonesia, 2010.
[33] M. Olivarius *et al.*, "Source and occurrence of radionuclides in geothermal water".
[34] T. Laier, *Vurdering af udfældningsricici ved geotermisk produktion fra Margretheholmboringen MAH-1A. Beregning af mætningsindeks for mineraler i saltvand fra Danmarks dybe undergrund*, vol. 2002. in Danmarks og Grønlands Geologiske Undersøgelse Rapport, no. 95, vol. 2002. GEUS, 2002. doi: 10.22008/gpub/18501.
[35] S. Chabab *et al.*, "Measurements and Modeling of High-Pressure O_2 and CO_2 Solubility in Brine (H_2O + NaCl) between 303 and 373 K and Pressures up to 36 MPa," *J. Chem. Eng. Data*, vol. 66, no. 1, pp. 609–620, Jan. 2021, doi: 10.1021/acs.jced.0c00799.

https://doi.org/10.26434/chemrxiv-2023-4hgnm **ORCID:** https://orcid.org/0000-0003-0475-323X Content not peer-reviewed by ChemRxiv. **License:** CC BY 4.0